1990ApJ...349..222T

THE ASTROPHYSICAL JOURNAL, 349:222–240, 1990 January 20
© 1990. The American Astronomical Society. All rights reserved. Printed in U.S.A.

EXPLOSIVE NUCLEOSYNTHESIS IN SN 1987A. II. COMPOSITION, RADIOACTIVITIES, AND THE NEUTRON STAR MASS

FRIEDRICH-KARL THIELEMANN
Harvard-Smithsonian Center for Astrophysics
MASA-AKI HASHIMOTO
Institut d'Astrophysique de Paris; Centre d'Etudes de Bruyeres-le-Chatel, Service de Physique et Techniques Nucleaires; and Service d'Astrophysique, CEN Saclay
AND
KEN'ICHI NOMOTO
Department of Earth Science and Astronomy, University of Tokyo
Received 1989 May 1; accepted 1989 July 13

ABSTRACT

We utilize the 20 $M_\odot$ model published by Nomoto and Hashimoto in 1988 with a 6 $M_\odot$ He core in order to perform explosive nucleosynthesis calculations. The employed explosion energy of 10^{51} ergs lies within the uncertainty range inferred from the bolometric light curve. The nucleosythesis processes and their burning products are discussed in detail. The results are compared with abundances from IR observations of SN 1987A and the average nucleosynthesis expected for Type II supernovae in Galactic chemical evolution. We predict the abundances of long-lived radioactive nuclei and their importance for the late light curve and gamma-ray observations. The position of the mass cut between the neutron star and the ejecta is deduced from the total amount of ejected ^{56}Ni (0.07 ± 0.01 $M_\odot$). This requires a neutron star with a baryonic mass $M_b = 1.6 \pm 0.045$ $M_\odot$, which corresponds to a gravitational mass $M_g = 1.43 \pm 0.05$ $M_\odot$ after subtracting the binding energy of a nonrotating neutron star. This uncertainty range only covers errors in the observed values of ^{56}Ni and the explosion energy; uncertainties of the stellar model could increase this value up to $M_b = 1.7$ $M_\odot$ and $M_g = 1.52$ $M_\odot$.

Subject headings: nucleosynthesis — stars: individual (SN 1987A) — stars: neutron — stars: supernovae

I. INTRODUCTION

SN 1987A was the first Type II supernova event in which one was able to identify the progenitor star, detect neutrinos from the core collapse, and measure the amount of ^{56}Ni from the light curve and known distance. It therefore is an excellent case to make contact between theoretical models and detailed observations, which hopefully will lead to a complete understanding of this specific supernova and Type II supernovae in general.

The constraints on the progenitor star of SN 1987A, Sk $-69°202$, come from optical observations (luminosity, color, and known distance) and give the following properties: $R = (3 \pm 1) = 10^{12}$ cm and a main-sequence mass $M_{MS} = 19 \pm 3$ $M_\odot$ (Shigeyama, Nomoto, and Hashimoto 1988; Woosley 1988). This corresponds to a star with a He core mass of 6 ± 1 $M_\odot$ after core hydrogen burning (Nomoto and Hashimoto 1988; Woosley and Weaver 1988). Several attempts have been made to explain the evolution of a 20 $M_\odot$ star which explodes as a blue supergiant. They include combinations of low metallicities in the LMC, mass loss, and helium enrichment of the H-rich envelope (Arnett 1987; Hillebrandt *et al.* 1987; Truran and Weiss 1987; Maeder 1987; Woosley 1988; Barkat and Wheeler 1988; Saio, Kato, and Nomoto 1988; Weiss 1989; Tuchman and Wheeler 1989).

Slow-moving nitrogen-rich material, detected in UV observations, has been interpreted as mass loss which the star underwent in a red giant stage less than 10,000–40,000 yr before its explosion (Casatella 1987; Kirshner 1988). Several arguments involving the observed light curve (Nomoto, Shigeyama, and Hashimoto 1987; Woosley, Pinto, and Ensman 1988; Shigeyama, Nomoto, and Hashimoto 1988; Woosley 1988; Grebenev and Sunyaev 1988; Arnett and Fu 1989), the H-envelope structure (Barkat and Wheeler 1988; Saio, Kato, and Nomoto 1988), and synthetic spectra (Höflich 1988) suggest a total mass loss between 3 and 7 $M_\odot$. An explosion energy of (0.7–1.6) $\times 10^{51}$ ergs is deduced from the early light curve. The late light curve, which shows an exponential decline, is powered by the decay of ^{56}Co and demands a total amount of 0.07 ± 0.01 $M_\odot$ of ^{56}Ni to be produced in the explosion (Shigeyama, Nomoto, and Hashimoto 1988; Woosley 1988; Arnett and Fu 1989). The production of ^{56}Ni has also been identified directly from gamma-ray lines with the *Solar Maximum Mission* satellite (*SMM*; Matz *et al.* 1988) and balloon flights (Mahoney *et al.* 1988; Sandie *et al.* 1988; Cook *et al.* 1988; Gehrels, Leventhal, and MacCallum 1988; Teegarden *et al.* 1989).

The most desirable way to perform explosive nucleosynthesis calculations would come from a hydrodynamical calculation, following the Fe core collapse, the bounce at nuclear densities, and the propagating shock wave through the envelope which will be ejected. However, there exist still open problems with the supernova mechanisms for a massive star like Sk $-69°202$. Both suggested Type II supernova mechanisms—the prompt and the delayed mechanism—have either problems to cause a successful explosion or the correct supernova energy. In either case, the hydrostatic evolution of a massive star ends with the collapse of the Fe core which proceeds to central densities in excess of nuclear densities. The gravitational binding energy of 2–3 $\times 10^{53}$ ergs, gained during the collapse, is released in form of blackbody neutrino radiation, which was actually observed for the case of SN 1987A by the Kamiokande II and IMB detectors (Hirata *et al.* 1987; Bionta *et al.* 1987).

© American Astronomical Society • Provided by the NASA Astrophysics Data System

1990ApJ...349..222T

The prompt mechanism relies on the shock wave which forms at the edge of the homologously collapsed core, after the transformation of nuclei into nucleons at nuclear densities. With typical values of the lepton concentration $Y_L = Y_e + Y_\nu = 0.38$ at bounce, this core has mass close to 0.84 $M_\odot$ and—somewhat dependent on the equation of state—a shock energy of about $E_s = 6.9(Y_L/0.4)^{10/3}[1 + (S_f^2/10)] \times 10^{51}$ ergs (Burrows and Lattimer 1983). Here Y_L is the lepton concentration at bounce and S_f is the entropy per baryon in units of k_B. Due to the dissociation of heavy nuclei into nucleons by the propagating shock front (8.7 MeV nucleon^{-1} = 8×10^{18} ergs g^{-1}) in the remainder of the initial Fe core, pure energy conservation requires Fe cores not larger than about 1.3 $M_\odot$. However, also neutrino transport leaks energy from the shock and the most recent calculations, including all three neutrino flavors and neutrino-electron scattering, quote maximum Fe core masses of 1.1–1.2 $M_\odot$ in order to ensure a prompt explosion (Bruenn 1989*a b*; Cooperstein and Baron 1989; Myra and Bludman 1989). The stellar evolution calculations of Nomoto and Hashimoto (1988) and Woosley and Weaver (1988) obtain an Fe core close to 1.4 $M_\odot$ for stars of approximately 20 $M_\odot$ and would therefore not support a prompt explosion with present input physics for SN 1987A. Mönchmeyer (1989) explored possible ways to rescue the prompt mechanism by including reasonable amounts of rotation (rotational to gravitational energy $\approx$0.01 at the onset of collapse) and could demonstrate a 50% increase of the shock energy in two-dimensional calculations, in comparison to the spherically symmetric case.

While all these phenomena occur on time scales of 30–50 ms, the delayed mechanism works on longer time scales. The gravitational binding energy of the collapsed proto–neutron star (2–3) $\times 10^{53}$ ergs is released in neutrinos, which have the shortest diffusion time scales of the order 0.5 to several seconds, depending on the neutrino energy. If neutrino heating converts less than 1% of the totally available energy into kinetic energy of the baryonic matter via neutrino captures and scattering, the typical supernova energy of (1–2) $\times 10^{51}$ ergs can still emerge. Delayed explosions have been modeled by Wilson (1986), Bethe and Wilson (1985), Wilson *et al.* (1986), Wilson and Mayle (1988), and Mayle and Wilson (1988). When these calculations are performed without convection, only explosion energies of a few times 10^{50} ergs are attained. However, the region of the stalled shock, with a gradient in electron concentration Y_e, is unstable with respect to the Saltfinger instability, causing convection which can enhance the explosion energy (Wilson and Mayle 1988; Mayle and Wilson 1988).

From the previous discussion it follows that at present the explosion mechanism is uncertain for 18–20 $M_\odot$ stars. The statistics of the observed neutrinos from SN 1987A is also not sufficient to distinguish between the two mechanisms mentioned here (Burrows 1988). Under these conditions, given the fact that an energy of (0.7–1.6) $\times 10^{51}$ ergs has been observed, several groups (Arnett 1987; Shigeyama *et al.* 1987; Woosley, Pinto, and Ensman 1988) modeled light curve calculations with an artificially induced shock wave of an intermediate energy. We follow the same approach for calculating the explosive nucleosythesis and employed the results of the spherical hydrocalculation by Shigeyama, Nomoto, and Hashimoto (1988) with a shock energy of 10^{51} ergs. This is actually the only method which has been used in the past for nucleosynthesis studies of Type II supernovae (see Woosley and Weaver 1986).

II. SHOCK PROPAGATION AND EXPLOSIVE PROCESSING

A shock wave which is strong enough to eject the outer mass zones and leaves a neutron star in the center increases temperatures and densities when passing through the Si, O, Ne, C, He, and H zones. Due to this temperature enhancement in the different burning shells during the passage of the shock wave, reactions which proceed already on long (evolutionary) time scales are accelerated by orders of magnitude and additional reactions become possible. The types of explosive nucleosynthesis processes are already discussed in great detail by Woosley, Arnett, and Clayton (1973). For similar processes in Type I supernovae, see Thielemann, Nomoto, and Yokoi (1986), and for a general overview of research carried out until 1986, see Woosley and Weaver (1986).

With the lack of self-consistent collapse and explosion calculations for 18–20 $M_\odot$ stars, which reproduce the observed explosion energies of (0.7–1.6) $\times 10^{51}$ ergs, we employed an artificially induced shock wave of intermediate energy and used the results of the spherical hydrocalculation by Shigeyama, Nomoto, and Hashimoto (1988) for the final kinetic energy of 1×10^{51} ergs. The only assumption, made implicitly by running a shock wave through the initial model, is that matter which is finally ejected did not experience significant changes between the onset of the collapse of the inner core and the arrival of the shock wave. The assumption that these layers did not experience any significant compression is well justified for the outer part of the Si shell by collapse calculations (E. Baron and M. Aufderheide, private communication).

Then the explosive nucleosynthesis can be performed easily. We take the stellar model with a 6 $M_\odot$ He core by Nomoto and Hashimoto (1988), which corresponds to an 17–20 $M_\odot$ star. Figure 1 shows the maximum temperatures and densities obtained for a shock energy of 10^{51} ergs in the calculations by Shigeyama, Nomoto, and Hashimoto (1988). For each mass zone we solve the coupled system of differential equations, governing the change of nuclear abundances $Y_i = n_i/(\rho N_A)$, with n_i being the number density of nucleus i and N_A Avogadro's number:

$$\dot{Y}_i = \sum_j c_j^i Y_j + \sum_{j,k} c_{j,k}^i Y_j Y_k + \sum_{j,k,l} c_{j,k,l}^i Y_j Y_k Y_l \,. \qquad (1)$$

The coefficients c^i in the three terms are related to different types of reaction rates: (1) decays, photodisintegrations, and electron captures λ_j; (2) two-particle reactions $\langle j, k\rangle$; and (3) three particle reactions $\langle j, k, l\rangle$ like the triple-alpha process, which can be interpreted as successive captures with an intermediate unstable target. The individual c^i's are given by $c_j^i = N_i \lambda_j$, $c_{j,k}^i = N_i/(N_j! N_k!)(\rho N_A)\langle j, k\rangle$, and $c_{j,k,l}^i = N_i/(N_j! N_k! N_l!)(\rho N_A)^2\langle j, k, l\rangle$. The N_i's can be positive or negative numbers and specify how many particles of species i are created or destroyed in a reaction and the denominators, including factorials, avoid double counting of the number of reactions when identical particles react with each other (for example, in the $^{12}C + {}^{12}C$ or the triple-alpha reaction). The present nucleosynthesis calculation employs reaction rates on light nuclei which are based on experimental information from Caughlan and Fowler (1988), Bao and Käppeler (1987), Wiescher *et al.* (1986, 1987, 1989), Wiescher, Görres, and Thielemann (1988), Wiescher (1989), and also from Wagoner (1969), and Wagoner, Fowler, and Hoyle (1967), if otherwise not available. For medium and heavy nuclei with higher nuclear level densities, the new statistical model rates by Thielemann, Arnould, and Truran (1987) are used. Weak interaction rates

© American Astronomical Society • Provided by the NASA Astrophysics Data System

1990ApJ...349..222T

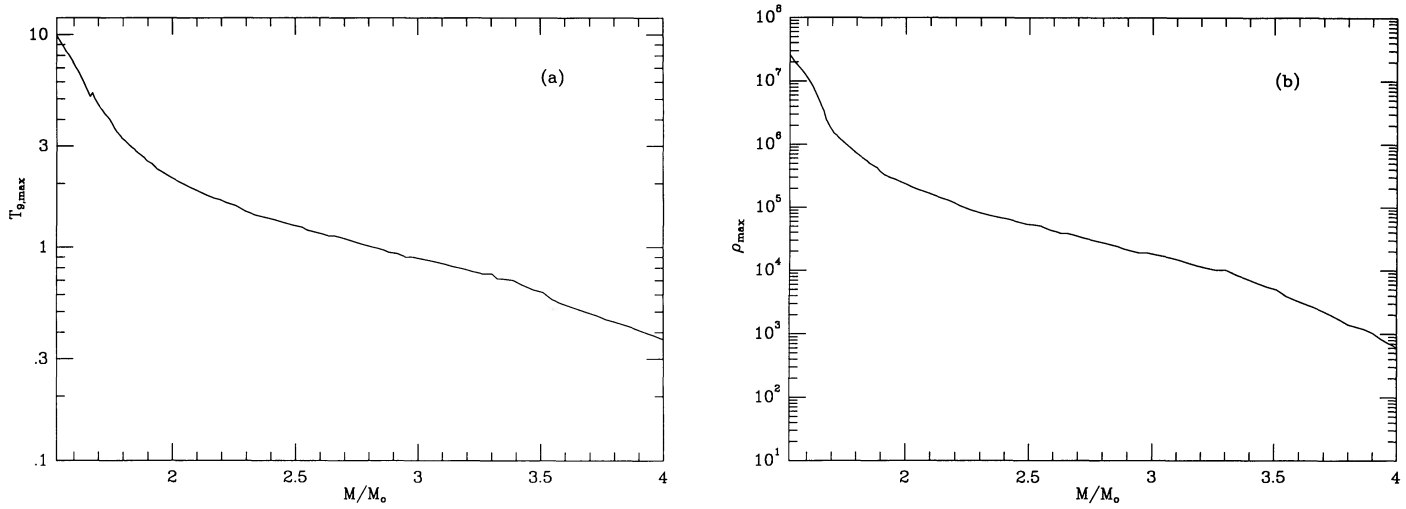

FIG. 1.—Maximum temperatures and densities attained in the inner part of the ejecta($1.6 < M/M_\odot < 4$), during the passage of a shock front with $E = 10^{51}$ ergs. Note that only matter inside 2 $M_\odot$ experiences temperatures in excess of 2×10^9 K.

are taken from Fuller, Fowler, and Newman (1980, 1982, 1985). Electron screening in the strong screening regime has been treated according to Itoh *et al.* (1979) and Alastuey and Jancovici (1978). In the weak and intermediate screening regime, the description of Graboske *et al.* (1973) was applied.

This calculation differs from an earlier one by Hashimoto, Nomoto, and Shigeyama (1989, hereafter Paper I; see also Nomoto *et al.* 1988) in two ways. We used a more extended network of 300 instead of 242 nuclei; especially more proton-rich nuclei were included in the Fe group. A list of these nuclei is given in Table 1A. A qualitative difference is that all statistical model reaction rates by Woosley *et al.* (1979) were replaced by new and improved rates (Thielemann, Arnould, and Truran 1987). These also include width fluctuation corrections; realistic optical potentials for neutrons, protons, and alpha particles; a macroscopic-microscopic treatment to predict resonance energies and widths of the giant dipole resonance (in order to calculate the gamma widths); and an improved treatment of the level density of excited states, still based on the backshifted Fermi gas model. The aim of the present work is to analyze the possible differences, resulting from the improved treatment, and to discuss the nucleosynthesis in SN 1987A in more detail. The hydrostatic phases of the presupernova evolution have been treated with a smaller network, containing 30 nuclei, including neutrons, for the burning phases from He- to O-burning and a network of 250 nuclei for the quasi-equilibrium and equilibrium phases of silicon burning (Nomoto and Hashimoto 1988). The members of the network of 30 nuclei are listed in Table 1B. More details will be given in Paper III (Hashimoto and Nomoto 1989), which deals mainly with the influence of uncertainties in stellar evolution on the presupernova model and the eventual supernova outcome.

We show a few major abundances resulting from the nucleosynthesis calculations in Figure 2 as a function of radial mass. In the innermost part of the ejecta ($M < 1.7\ M_\odot$), where explosive Si-burning with Si exhaustion takes place, ^{56}Ni is the dominant nucleus. The abundance changes by almost a factor of 2 at $M = 1.63\ M_\odot$. This coincides exactly with the position where the electron concentration $Y_e = \sum_i Z_i\, Y_i$ changes from 0.494 to 0.499 (see Fig. 3). This decrease in Y_e has the effect that ^{56}Ni shares its abundance with more neutron-rich nuclei like ^{57,58}Ni and ^{61,62}Zn. Contrary to Type I supernovae, where high densities cause large electron Fermi energies and lead to substantial electron captures during explosive processing, the Y_e in Figure 3 is identical to that of the precollapse model. In the mass zones beyond 1.7 $M_\odot$ incomplete Si-burning and explosive O-burning produce ^{28}Si, ^{32}S, ^{36}Ar, and ^{40}Ca. Explosive Ne-burning enhances mostly ^{16}O and produces also ^{24}Mg and ^{28}Si. Explosive C-burning seems negligible and material beyond 2 $M_\odot$ is ejected essentially unaltered by explosive processing. In order to accommodate the observed ^{56}Ni mass of 0.07 $M_\odot$ in the ejecta, one has to place the mass cut between the ejecta and the remaining neutron star at 1.6 $M_\odot$.

For comparison we also show the composition of the same mass zones before core collapse and the outward propagation of the shock front in Figure 4. It can be seen that the zones beyond 1.6 $M_\odot$, which will be ejected, contain only products of H-, He-, C-, Ne-, and O-burning. The boundary of O-burning is located at 1.67 $M_\odot$. The drop in Y_e at 1.63 $M_\odot$ corresponds to a change in the neutron excess $\eta = \sum_i (N_i - Z_i)Y_i/$

TABLE 1A

NUCLEI IN FULL NETWORK

n	$^{1-3}$H	^{3,4,6}He	$^{6-8}$Li
$^{7,9-11}$Be	$^{8,10-12}$B	$^{10-15}$C	$^{12-17}$N
$^{14-20}$O	$^{17-21}$F	$^{18-25}$Ne	$^{20-26}$Na
$^{21-28}$Mg	$^{23-30}$Al	$^{25-33}$Si	$^{27-35}$P
$^{29-38}$S	$^{31-40}$Cl	$^{33-44}$Ar	$^{35-46}$K
$^{37-49}$Ca	$^{40-50}$Sc	$^{42-52}$Ti	$^{44-54}$V
$^{46-56}$Cr	$^{48-58}$Mn	$^{50-62}$Fe	$^{52-63}$Co
$^{54-67}$Ni	$^{57-69}$Cu	$^{59-72}$Zn	$^{61-74}$Ga
$^{68-78}$Ge			

TABLE 1B

HYDROSTATIC NETWORK

n	^{1}H	^{4}He	^{12}C
^{14}N	^{16,18}O	$^{20-22}$Ne	^{23}Na
$^{24-26}$Mg	$^{26-27}$Al	$^{28-30}$Si	$^{30-31}$P
$^{31-34}$S	^{35}Cl	^{36,38}Ar	^{39}K
^{40}Ca			

© American Astronomical Society • Provided by the NASA Astrophysics Data System

1990ApJ...349..222T

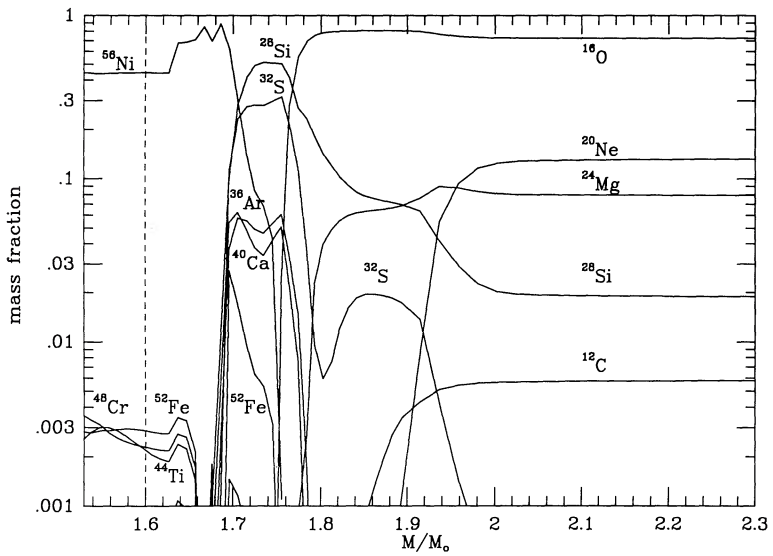

FIG. 2.—Mass fractions of a few major nuclei, as they result from explosive processing after the passage of the supernova shock front. Matter outside 2 $M_\odot$ is essentially unaltered (see Fig. 4). Zones further in experience explosive Ne, O, and Si-burning. Inside 1.7 $M_\odot$, Fe group nuclei dominate. The drop in the ^{56}Ni abundance at $M = 1.63\ M_\odot$ coincides with a change in Y_e, which favors more neturon-rich nuclei in the innermost part of the ejecta. The dashed line indicates the position of the mass cut, if only 0.07 $M_\odot$ of ^{56}Ni should be ejected.

$\sum_i A_i Y_i = 1 - 2Y_e$ from 2×10^{-3} to 1.2×10^{-2}. This position marks the outer boundary of the O-burning convective shell which extends from 1.05 to 1.63 $M_\odot$ after exhaustion of oxygen in the central region. Because of larger abundances of silicon-rich products and higher densities, this layer undergoes more electron captures than the outer layers during oxygen-shell burning and the subsequent contraction of the Si-rich core. This layer also contains traces of neutron-rich material which was convectively mixed in from the Si-burning shell. The layers from 1.63 to 1.67 $M_\odot$ mark the propagation of the O-burning shell, which operated at lower densities than shell burning at 1.05 $M_\odot$ and did not experience electron captures. Thus $\eta = 2 \times 10^{-3}$ has the average value after core He-, C-, and Ne-burning (see Fig. 7 in Thielemann and Arnett 1985). The comparison between Figures 2 and 4 makes clear that nuclei heavier than Ar, which are ejected in the supernovae explosion, are entirely due to explosive processing. In the hydrostatic layers beyond 1.6 $M_\odot$ only products of hydrostatic H-, He-, C-, Ne-, and O-burning are existing. As stated before, the position of the O-burning shell is at 1.67 $M_\odot$, the convective C- and Ne-burning shell extends out to 3.7 $M_\odot$. Explosive burning in the propagating shock front then creates new positions of the burning shells. Si-burning moves out to 1.74 $M_\odot$, O-burning to 1.8 $M_\odot$, and combined Ne-burning and C-burning to 2 $M_\odot$. Material beyond 2 $M_\odot$ is essentially unaltered by the propagating shock front.

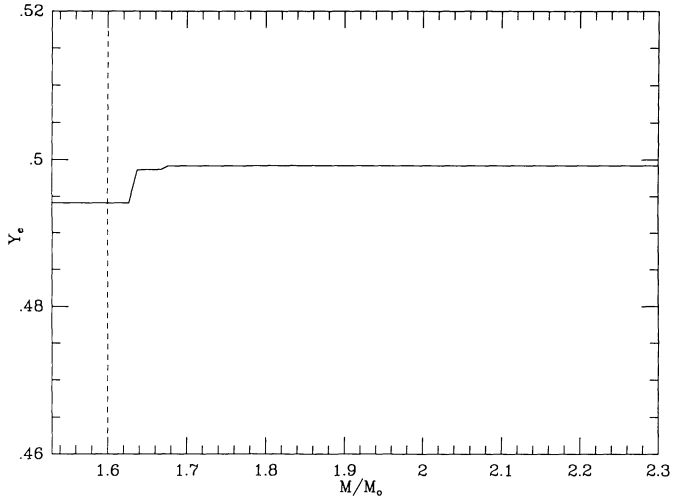

FIG. 3.—Electron abundance Y_e as a function of radial mass. The drop at 1.63 $M_\odot$ reflects the outer boundary of the Si zone which experienced core O-burning and admixtures of Si shell burning during hydrostatic evolution. The position of the mass cut, with respect to this change in Y_e, is crucial for the composition of Fe group elements.

This result was obtained by performing the shock wave calculation for only one energy in the allowed range. A higher energy would move the mass cut to slightly larger masses, when meeting the requirement that only 0.07 $M_\odot$ of ^{56}Ni should be ejected. This would also reduce the neutron excess of matter in the innermost ejected zones. In addition, the sensitivity to the stellar model has to be explored. One of the major free parameters in stellar evolution is the still uncertain $^{12}C(\alpha, \gamma)^{16}O$ reaction (see Filippone, Humblet, and Langanke 1989; Caughlan *et al.* 1985; and Caughlan and Fowler 1988). The new measurements by Kremer *et al.* (1988) agree essentially with earlier experiments by Kettner *et al.* (1982) and Redder *et al.* (1987). The open and still unresolved problem lies in the extrapolation to low energies ($\approx$300 keV), which are of importance for hydrostatic helium burning. The present calculation was performed with the rate of Caughlan *et al.* (1985). The discussion of the results will show later that this seems to be a choice consistent with existing abundance observations of SN 1987A.

III. INDIVIDUAL BURNING PROCESSES

a) Explosive Si-*Burning*

Zones which experience temperatures in excess of 4.0–5.0 $\times 10^9$ K undergo explosive Si-burning. Temperatures beyond 5×10^9 K lead to complete Si exhaustion and produce only Fe group nuclei. From Figure 1 we notice that this limit is

© American Astronomical Society • Provided by the NASA Astrophysics Data System

1990ApJ...349..222T

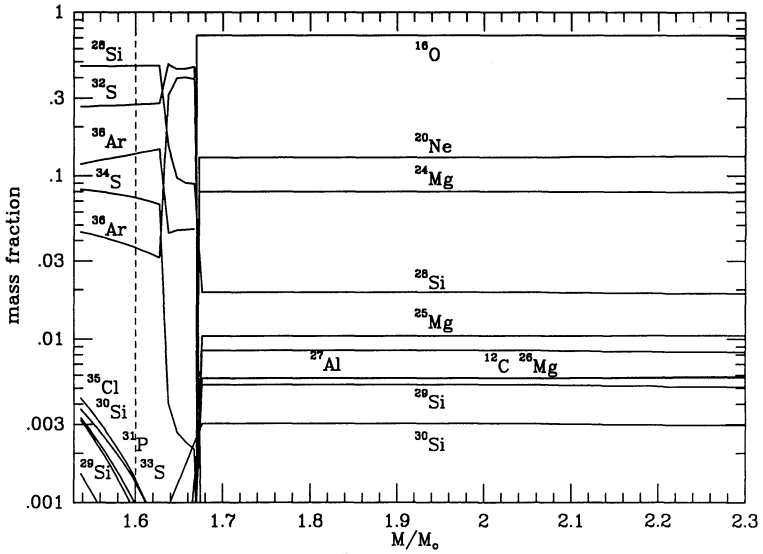

FIG. 4.—Mass fractions of major nuclei, resulting from hydrostatic burning stages prior to core collapse. Displayed are the zones which will later be ejected by the propagating shock front. It is seen that no elements heavier than Ar are contained in these zones.

located at 1.7 $M_\odot$, consistent with the results displayed in Figure 2. A simplified analytical calculation leads to the same outcome. Weaver and Woosley (1980) already recognized that matter behind the shock front is strongly radiation dominated. Assuming an almost homogeneous density and temperature distribution behind the shock (which is approximately correct; see Fig. 3 in Shigeyama, Nomoto, and Hashimoto 1988), one can equate the supernovae energy with the radiation energy inside the radius R of the shock front

$$E_{SN} = \frac{4\pi}{3} R^3 a T^4 . \quad (2)$$

This equation can be solved for R and with $T = 5 \times 10^9$ K and $E_{SN} = 10^{51}$ ergs, the result is $R \approx 3500$ km (see Woosley 1988). For the evolutionary model by Nomoto and Hashimoto (1988), utilized in this calculation, this radius corresponds to 1.7 $M_\odot$, in excellent agreement with the exact hydrodynamical calculation.

Explosive Si-burning can be divided into three different regimes: incomplete Si-burning and complete Si-burning with Si exhaustion, undergoing either a normal or alpha-rich freeze-out. Which of the three regimes is encountered depends on the peak temperatures and densities attained during the passage of the shock front (see Fig. 20 in Woosley, Arnett, and Clayton 1973, and Fig. 5 in Thielemann, Nomoto, and Yokoi 1986). In complete Si-burning the abundances follow a nuclear statistical equilibrium (NSE) during explosive processing and they are only determined by the nuclear binding energies, partition functions, temperatures, and densities. The NSE can also be sustained when the expansion leads to decreasing temperatures until the freeze-out of charged particle reactions. Then the final composition corresponds to the NSE abundances at freeze-out conditions. Such a normal freeze-out occurs at high densities, when the strongly density dependent triple-alpha reaction can burn ^{4}He to heavier nuclei in phase with the temperature decrease, which favors heavy nuclei and less free alpha particles. At lower densities this cannot be achieved anymore and an alpha-rich freeze-out occurs, which distorts the NSE abundances of heavy nuclei by additional alpha-captures. Figure 5 shows the position of mass zones which experience explosive Si-burning in the peak temperature and density plane. We notice that only alpha-rich freeze-out and incomplete Si-burning are encountered. Contrary to Type I supernovae (see Fig. 5 in Thielemann, Nomoto, and Yokoi 1986), densities in excess of 10^8 g cm^{-3}, which would result in a normal freeze-out are not attained in the ejecta. The region which experiences incomplete Si-burning starts at 1.69 $M_\odot$.

The most abundant nucleus in the normal and alpha-rich freeze-out is ^{56}Ni, in case the neutron excess is smaller than 2×10^{-2} or Y_e is larger than 0.49, which is fulfilled even for the innermost ejecta in our calculation. For the less abundant nuclei, the final alpha-capture plays a dominant role transforming nuclei like ^{56}Ni, ^{57}Ni, and ^{58}Ni into ^{60}Zn, ^{61}Zn, and ^{62}Zn. This is shown in Figure 6 which displays the abundances

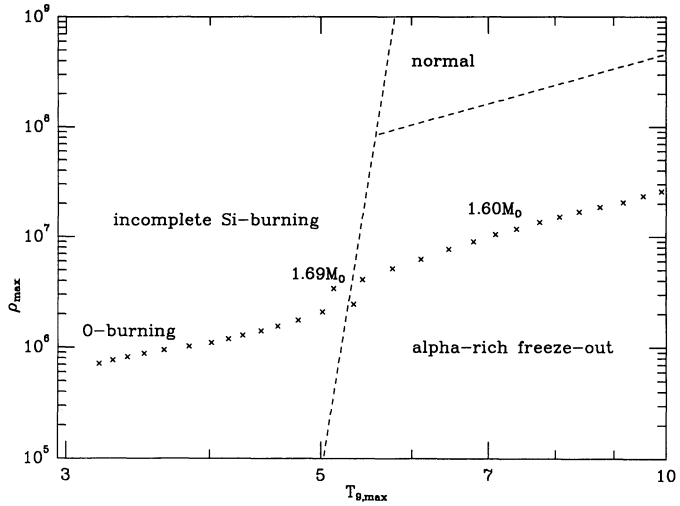

FIG. 5.—Peak temperatures and densities of the innermost mass zones ejected in the supernova explosion. Each point marks the conditions for one mass zone. The dashed lines divide the areas of normal and alpha-rich freeze out and incomplete Si-burning. The innermost mass zones undergo alpha-rich freeze-out.

© American Astronomical Society • Provided by the NASA Astrophysics Data System

1990ApJ...349..222T

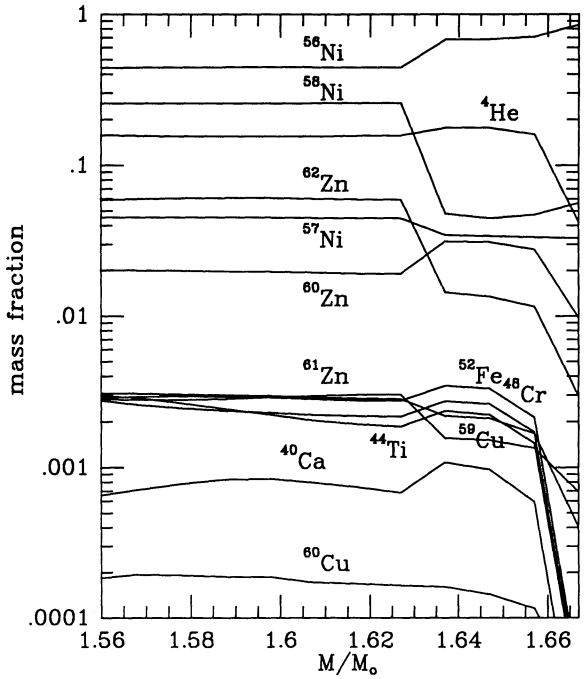

FIG. 6.—Mass fractions of the dominant nuclei in zones which experience alpha-rich freeze-out. Notice the relatively large amounts of Zn and Cu nuclei, which originate from alpha captures on Ni and Co. One can recognize their strong decrease beyond 1.66 $M_\odot$, which goes parallel with the decrease of the ^{4}He abundance and other alpha-nuclei like ^{40}Ca, ^{44}Ti, ^{48}Cr, and ^{52}Fe. Nuclei which would dominate in a nuclear statistical equilibirum like $^{56, 57, 58}$Ni stay constant or increase even slightly. The increase of all nuclei with $N = Z$ at 1.63 $M_\odot$ and the decrease of nuclei with $N > Z$ is due to the change in Y_e (see Fig. 3).

of nuclei for the mass zones of alpha-rich freeze-out. In addition, one can verify the fact that a too slow triple-alpha reaction which still continues to produce ^{12}C, when the NSE would already require to concentrate all abundances in heavier nuclei, leads to the production of trace abundances of ^{40}Ca, ^{44}Ti, ^{48}Cr, and ^{52}Fe. It also shows how the abundances of these latter nuclei and ^{60}Zn, ^{61}Zn, and ^{62}Zn decrease with a declining mass fraction of alpha particles. The ^{4}He mass fraction in these zones reaches values of 16%–18%. The increase of Y_e at 1.63 $M_\odot$ favors the less neutron-rich nuclei.

Incomplete Si-burning extends out to 1.74 $M_\odot$ and is characterized by peak temperatures of 4–5 $\times$ 10^9 K. Temperatures are not high enough for an efficient bridging of the bottleneck above the proton magic number $Z = 20$ by nuclear reactions. Therefore no complete NSE is attained. Instead only a partial equilibrium (quasi equilibrium = QSE) for the relative abundances of nuclei in each of the two QSE groups $Z \leq 20$ and $Z > 20$ is obtained, while the total ratio between both groups is out of equilibrium (Woosley, Arnett, and Clayton 1973; Thielemann and Arnett 1985). Besides the dominant fuel nuclei ^{28}Si and ^{32}S we find the alpha-nuclei ^{36}Ar and ^{40}Ca as most abundant members of the lower QSE group. Partial leakage into the QSE group around Fe produces ^{56}Ni and ^{54}Fe as dominant abundances. Smaller amounts of ^{52}Fe, ^{58}Ni, ^{55}Co, and ^{57}Ni are encountered. The detailed composition for the zones undergoing incomplete Si-burning in the mass range $1.69 < M/M_\odot < 1.74$ is displayed in Figure 7, together with the products of explosive O-burning.

b) Explosive Oxygen Burning

Temperatures in excess of roughly 3.3 $\times$ 10^9 K lead to a quasi equilibrium in the lower QSE cluster which extends over the range $28 < A < 45$ in mass number (Woosley, Arnett, and Clayton 1973). These conditions are accomplished in explosive O-burning in the mass zones up to 1.8 $M_\odot$. The main burning products are ^{28}Si, ^{32}S, ^{36}Ar, ^{40}Ca, ^{38}Ar, and ^{34}S. With mass fractions less than 10^{-2} also, ^{33}S, ^{39}K, ^{35}Cl, ^{42}Ca, and ^{37}Ar show up. In the innermost zones with temperatures close to 4 $\times$ 10^9 K, there exists still a contamination by the Fe group nuclei ^{54}Fe, ^{56}Ni, ^{52}Fe, ^{58}Ni, ^{55}Co, and ^{57}Ni, as shown in Figure 7. The abundaces in the QSE cluster are determined by alpha, neutron, and proton abundances. Because electron capture during explosive processing is negligible, the original neutron excess stays unaltered and fixes the neutron to proton ratio. Under those conditions the resulting composition is

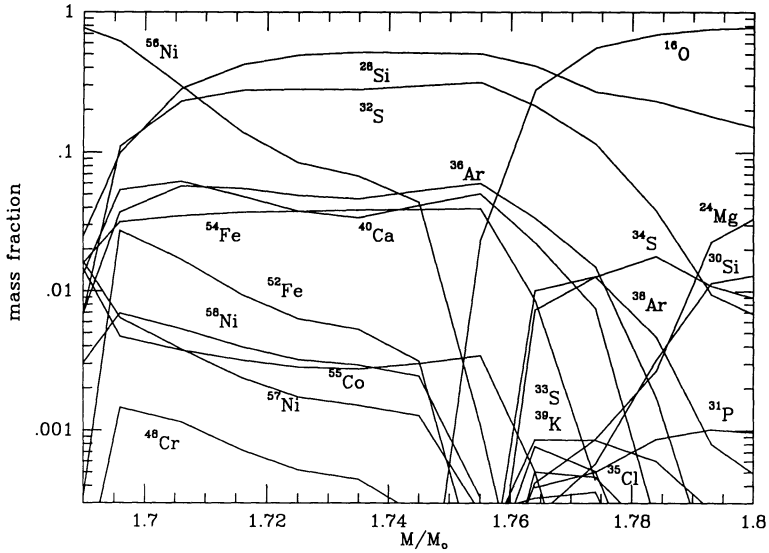

FIG. 7.—Mass fractions of nuclei in the zones of incomplete Si-burning $M < 1.74$ $M_\odot$ and explosive O-burning $M < 1.8$ $M_\odot$. The Si-burning zones are characterized by important quantities of Fe group nuclei besides ^{28}Si, ^{32}S, ^{36}Ar, and ^{40}Ca. Explosive O-burning produces mostly the latter, together with more neutron-rich nuclei like ^{30}Si, ^{34}S, ^{38}Ar, etc.

© American Astronomical Society • Provided by the NASA Astrophysics Data System

1990ApJ...349..222T

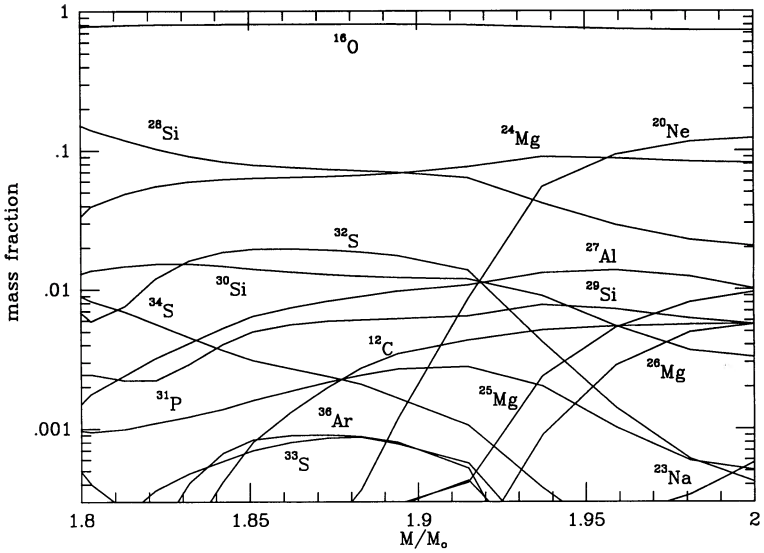

FIG. 8.—Composition in mass zones of explosive Ne- and C-burning. The dominant products are ^{16}O, ^{24}Mg, and ^{28}Si. Besides the major abundances, mentioned above, explosive neon burning supplies also substantial amounts of ^{27}Al, ^{29}Si, ^{32}S, ^{30}Si, and ^{31}P. Explosive carbon burning contributes in addition the nuclei ^{20}Ne, ^{23}Na, ^{24}Mg, and ^{26}Mg.

dependent only on the alpha to neutron ratio at freeze-out. Woosley, Arnett, and Clayton (1973) pointed out already that with a neutron excess of 2×10^{-3} the solar ratios of ^{39}K/^{35}Cl, ^{40}Ca/^{36}Ar, ^{36}Ar/^{32}S, ^{37}Cl/^{35}Cl, ^{38}Ar/^{34}S, ^{42}Ca/^{38}Ar, ^{41}K/^{39}K, and ^{37}Cl/^{33}S are attained within a factor of 2 for freeze-out temperatures in the range $(3.1–3.9) \times 10^9$ K. This is the typical neutron excess resulting from solar CNO abundances, which are first transformed into ^{14}N in H-burning and then into ^{22} Ne in He-burning via ^{14}N$(\alpha, \gamma)^{18}$F$(\beta^+)^{18}$O$(\alpha, \gamma)^{22}$Ne. In stars with lower metallicities, these ratios will drop accordingly. The comparison of these abundances to solar values will be discussed in § V.

c) *Explosive Neon and Carbon Burning*

The main burning products of explosive neon burning are ^{16}O, ^{24}Mg, and ^{28}Si, synthesized via the reaction sequences ^{20}Ne$(\gamma, \alpha)^{16}$O and ^{20}Ne$(\alpha, \gamma)^{24}$Mg$(\alpha, \gamma)^{28}$Si, similar to the hydrostatic case. The ^{16}O enhancement over its hydrostatic value, caused by this mechanism in the mass zones up to 2 $M_\odot$, can be seen in Figure 8. The mass zones in question have peak temperatures in excess of 2.1×10^9 K. They undergo a combined version of explosive neon and carbon burning. Besides the major abundances, mentioned above, explosive neon burning supplies also substantial amounts of ^{27}Al, ^{29}Si, ^{32}S, ^{30}Si, and ^{31}P. Explosive carbon burning contributes in addition the nuclei ^{20}Ne, ^{23}Na, ^{24}Mg, ^{25}Mg, and ^{26}Mg.

d) *r-Process Nuclei*

i) *Neutron-rich Zones Close to the mass Cut*

The most neutron-rich zones of the ejecta are located at the inner boundary around 1.60 $M_\odot$ with a Y_e of 0.494 which corresponds to a neutron excess $\eta = \sum_i (N_i - Z_i) Y_i / \sum_i A_i Y_i = 1–2Y_e$ of 1.2×10^{-2}. These zones which experience temperatures in excess of 5×10^9 K, produce predominantly nuclei in the mass range 50–60. The quoted value of η therefore indicates that each nucleus has about 0.5 more neutrons than protons. For that mass region this corresponds to a nucleus being about 1.5 mass units more proton-rich than the stability line. The operation of an *r*-process is, however, characterized by the fact that, after the freeze-out of charged particle reactions, 10–100 neutrons per heavy nucleus have to be available for the onset of substantial neutron capture. Such conditions exist only in matter which was compressed to densities of 10^{11}–10^{12} g cm^{-3}, undergoing electron captures until a beta equilibrium is attained (Cameron 1989). This beta equilibrium produces nuclei with Q-values for β^- decay equal to the electron Fermi energy (Lattimer *et al.* 1977; Shapiro and Teukolsky 1983) of about 34 MeV. In our calculation the matter in the innermost zones of the ejecta close to 1.6 $M_\odot$, experienced only densities up to 10^7 g cm^{-3} during the propagation of the shock front and therefore cannot meet this requirement. This leads to the conclusion that no *r*-process material is ejected from zones close to the mass cut between neutron star and ejecta.

Such a conclusion relies on the assumption that rotation is not strong enough to violate spherical symmetry, which could cause jet like ejection at the poles (LeBlanc and Wilson 1970; Symbalisty, Schramm, and Wilson 1985). For reasonable ratios of rotational to gravitational energy of 1% before collapse, Mönchmeyer (1989) finds small jetlike circulations at the poles when the shock front is still close to the collapsed core but obtains an almost spherical symmetry when the shock front reaches the Si zone.

ii) *Explosive* He-*burning*

A different situation surfaces when the maximum temperatures are below freeze-out conditions for charged particle reactions with Fe group nuclei. Then reactions among light nuclei which release neutrons, like (α, n) reactions on ^{13}C and ^{22}Ne, can sustain a neutron flux. Existing heavy nuclei, with neutron cross sections which are much larger than for light and intermediate nuclei, will be the preferred targets for a neutron capture process. The constraint of having 10–100 neutrons per heavy nucleus, in order to attain *r*-process conditions, can then be met by small abundances of Fe group nuclei. Such conditions were expected when the shock front passes the He-burning shell and enhances the ^{22}Ne(α, n) reaction by orders of

© American Astronomical Society • Provided by the NASA Astrophysics Data System

1990ApJ...349..222T

magnitude (Truran, Cowan, and Cameron 1978; Thielemann, Arnould, and Hillebrandt 1979). Shorter beta-decay half-lives (Klapdor *et al.* 1981) seemed to make this scenario even more likely (Hillebrandt *et al.* 1981). Finally, however, Blake *et al.* (1981) and Cowan, Cameron, and Truran (1983) could show that this neutron source is not strong enough for an *r*-process in realistic stellar models. We do find the same result in our present calculations. Recent research based on additional neutron release via inelastic neutrino scattering (Epstein, Colgate, and Haxton 1988) can also not produce neutron densities of 10^{19}–10^{20} cm^{-3}, which are required for such a process to operate (see also Woosley *et al.* 1990).

This leads to the conclusion that a 20 $M_\odot$ star does not eject *r*-process nuclei in its final supernova explosion. Although Type II supernovae are strongly expected to be the dominant *r*-process source, this conclusion is in agreement with recent galactic chemical evolution studies based on observations of the Eu/Fe ratio in very metal-poor stars. A drop is found at [Fe/H] below -2.7 dex and interpreted in such a way that only Type II supernovae with masses less than 11 $M_\odot$ contribute to the observed *r*-process abundances (Mathews and Cowan 1989). These stars have longer lifetimes than more massive stars and would therefore only contribute to Galactic chemical evolution after a certain delay time, which corresponds to a metallicity of [Fe/H] of -2.7.

IV. QUANTITATIVE COMPOSITION OF THE EJECTA

a) Results

Tables 2 and 3 summarize the abundances in the ejecta of a 6 $M_\odot$ He core in units of $M_\odot$. The inner 1.59 $M_\odot$ (baryonic) of the neutron star are excluded and also the H-rich envelope. The exclusion of the latter has two reasons. First, the total envelope mass is known only within the limits of 7–11 $M_\odot$, from comparisons of the observed light curve with hydrodynamical calculations, including radiation transport (Shigeyama, Nomoto, and Hashimoto 1988; Woosley 1988; Arnett and Fu 1989). Second, the exact envelope composition is not known, but He enrichment is observed in metal-poor blue supergiants (Kudritzki *et al.* 1987) and utilized to explain the blue-red-blue transition (Saio, Kato, and Nomoto 1988; Barkat and Wheeler 1988). As a first test we want to compare Table 3 with the results of Hashimoto, Nomoto, and Shigeyama (1989, Paper I). They performed essentially the same calculation, using the same stellar model, explosion energy, and mass cut. There are only two differences with respect to the present work. The shock propagation and explosive processing was followed further out while it was neglected beyond 2.5 $M_\odot$ in Paper I. This should have no major effect on explosive nucleosynthesis as we showed that conditions for explosive C-, Ne-, O-, Si-burning are not met outside 2 $M_\odot$ and matter is ejected essentially unaltered. However, explosive He-burning can still affect light nuclei, predominantly nuclei lighter than Ne. We also made use of an updated data base of nuclear reactions, mainly by replacing the reaction rates for medium and heavy nuclei by Woosley *et al.* (1979) with the improved statistical model rates by Thielemann, Arnould, and Truran (1987). Nuclei with abundances which differ by less than a factor of 1.3 from Table 1 of Paper I are marked by a 0, nuclei different by more than a factor of 1.3 are marked by a 1, and nuclei different by more than a factor of 2 are identified by a 3. Among light nuclei we see a few major differences for ^{13}C, ^{15}N, ^{17}O, and ^{19}F. The reason for these discrepancies lies in the further propagation of the shock wave and our usage of updated reaction rates for proton-rich light nuclei by Wiescher *et al.* (1986, 1987), Wiescher, Görres, and Thielemann (1988), Wiescher *et al.* (1989), and Wiescher (1989).

Heavier nuclei are only affected by the change to the statistical model rates of Thielemann, Arnould, and Truran (1987). For the majority of nuclei the difference is small. Only the abundances of two nuclei (^{48}Ca and ^{64}Ni) differ by more than a factor of 3. Almost all nuclei which show changes by more than a factor of 1.3 (^{36}S, ^{40}Ar, ^{39,41}K, $^{42-44,46,48}$Ca, ^{45}Sc, ^{46,47,49,50}Ti, ^{51}V, ^{54}Cr, ^{59}Co, ^{64}Ni, ^{63,65}Cu, and ^{68}Zn) are located within two units of the magic numbers $N = 20$, $Z = 20$, $N = 28$, and $Z = 28$. This is expected because one of the major improvements in Thielemann, Arnould, and Truran (1987) was the treatment of level densities at magic numbers. They found that capture cross sections could be predicted within a factor of 2, while the rates by Woosley *et al.* (1979) could deviate up to a factor of 3–5, when the theoretical level densities were used for nuclei at magic numbers. Woosley *et al.* (1979) used experimental level densities whenever available, which assured a better agreement for reactions on stable nuclei. But explosive nucleosynthesis encounters a large number of unstable nuclei where this information is lacking. Therefore deviations for these nuclei by a factor of 2–3 are expected and consistent with the utilization of the improved reaction rates. Only three of the deviating nuclei (^{69}Ga, ^{72,73}Ge) are located further than two units from closed shells, but they are products of alpha-capture reactions from nuclei within these boundaries, during the alpha-rich freeze-out. Thus their abundances are consistent with the previous conclusions. Having these differences in mind, the comparison shows actually an excellent agreement between Paper I and this calculation and presents an important test for the accuracy involved. The comparison shows also that in applications of explosive nucleosynthesis the uncertainties of reaction rates are reflected in similar uncertainties of nuclear abundances. The results are much less sensitive to individual rates as encountered for major reactions in hydrostatic burning [e.g., ^{12}C(α, γ)^{16}O], where the fuel composition of subsequent burning stages can be altered drastically.

Before comparing the predicted abundances to observations of SN 1987A and other calculations of similar nature (Woosley, Pinto, and Weaver 1988), we want to point out the following. The postprocessing with a large network of 300 nuclei was performed only for the phases of explosive nucleosynthesis, i.e., during the passage of the supernova shock front. The hydrostatic phases of the presupernova evolution were covered by Nomoto and Hashimoto (1988) with a smaller network, containing 30 nuclei, for the phases from He-burning through O-burning and a quasi-equilibrium network containing 250 nuclei for Si-burning. The initial abundance of ^{26}Al was set to zero due to its short half-life at temperatures $> 6 \times 10^8$ K. The previous discussion also explains why nuclei which were produced in small amounts during hydrostatic burning stages and not included in the network of 30 nuclei are not treated correctly. This does not have any importance for the mass zones with $M < 2\ M_\odot$, where explosive processing leaves the dominant signature. However, the mass zones beyond 2 $M_\odot$ are altered by the shock front in a minor way and the abundances are almost entirely due to hydrostatic burning. Mostly affected by this shortening are light nuclei with small abundances (^{13}C, ^{15}N, ^{17}O, and ^{19}F) and (neutron-rich) *s*-process nuclei between Ne and the Fe group (e.g., ^{36}S, ^{37}Cl, ^{40}Ar, ^{40}K, ^{46,48}Ca, ^{50}Ti, ^{54}Cr, ^{58}Fe, and ^{64}Ni; see Arnett and Thielemann 1985).

© American Astronomical Society • Provided by the NASA Astrophysics Data System

1990ApJ...349..222T

TABLE 2

COMPOSITION OF EJECTA AFTER EXPLOSIVE PROCESSING, MASS CUT AT 1.59 $M_\odot$

	$M/M_\odot$		$M/M_\odot$		$M/M_\odot$		$M/M_\odot$		$M/M_\odot$
d	3.40E-17	t	1.08E-20	he3	1.35E-19	he4	2.10E+00	li6	5.10E-19
li7	4.42E-20	be7	7.39E-22	be9	7.64E-18	be10	1.46E-21	b10	2.73E-17
b11	6.35E-16	b12	4.86E-24	c11	1.17E-17	c12	1.14E-01	c13	4.46E-07
c14	7.39E-09	c15	1.52E-14	n13	7.90E-11	n14	2.71E-03	n15	4.39E-08
n16	4.49E-13	n17	1.04E-18	o14	4.08E-18	o15	1.79E-11	o16	1.48E+00
o17	3.73E-09	o18	8.68E-03	o19	7.09E-10	o20	1.45E-13	f17	5.24E-15
f18	2.41E-08	f19	1.54E-10	f20	4.65E-13	f21	9.55E-16	ne18	3.08E-23
ne19	5.30E-16	ne20	2.28E-01	ne21	3.02E-04	ne22	2.93E-02	ne23	1.62E-07
ne24	1.52E-12	ne25	2.55E-18	na21	2.50E-12	na22	1.01E-07	na23	1.17E-03
na24	2.01E-08	na25	3.21E-12	na26	1.43E-18	mg22	1.30E-16	mg23	4.33E-07
mg24	1.47E-01	mg25	1.84E-02	mg26	1.71E-02	mg27	8.40E-09	mg28	3.16E-12
al24	2.69E-22	al25	1.73E-10	al26	6.77E-06	al27	1.59E-02	al28	6.33E-06
al29	1.47E-08	al30	4.81E-14	si26	1.09E-14	si27	2.64E-07	si28	8.43E-02
si29	9.70E-03	si30	7.25E-03	si31	1.21E-06	si32	1.89E-09	si33	1.24E-17
p28	2.14E-23	p29	2.66E-10	p30	5.22E-05	p31	1.13E-03	p32	5.59E-07
p33	3.68E-07	p34	1.20E-11	p35	5.54E-14	s30	1.22E-14	s31	2.51E-08
s32	2.49E-02	s33	1.14E-04	s34	1.11E-03	s35	2.49E-07	s36	2.41E-07
s37	1.54E-16	s38	6.04E-18	cl32	3.02E-22	cl33	1.33E-11	cl34	3.81E-09
cl35	5.13E-05	cl36	5.42E-07	cl37	5.75E-07	cl38	6.90E-12	cl39	6.09E-14
cl40	4.48E-18	ar34	6.96E-15	ar35	3.45E-09	ar36	4.10E-03	ar37	5.66E-06
ar38	3.08E-04	ar39	1.59E-09	ar40	1.77E-09	ar41	2.07E-13	ar42	2.43E-15
ar43	1.79E-19	ar44	1.11E-21	k36	1.98E-19	k37	6.23E-13	k38	2.52E-07
k39	2.90E-05	k40	7.00E-09	k41	1.98E-09	k42	7.76E-12	k43	2.22E-13
k44	2.29E-15	k45	6.72E-17	k46	2.45E-19	ca38	1.07E-17	ca39	1.29E-09
ca40	3.31E-03	ca41	2.28E-06	ca42	9.79E-06	ca43	8.09E-09	ca44	4.23E-09
ca45	3.51E-12	ca46	2.93E-12	ca47	2.78E-15	ca48	3.97E-17	ca49	2.60E-25
sc40	8.86E-23	sc41	6.56E-15	sc42	4.59E-10	sc43	2.80E-06	sc44	2.41E-09
sc45	5.05E-09	sc46	3.49E-11	sc47	5.44E-12	sc48	4.90E-14	sc49	9.01E-16
sc50	4.06E-22	ti42	1.33E-25	ti43	2.57E-12	ti44	2.09E-04	ti45	1.84E-07
ti46	3.66E-06	ti47	8.14E-08	ti48	2.27E-08	ti49	6.48E-11	ti50	4.72E-11
ti51	2.88E-17	ti52	6.33E-21	v44	2.37E-23	v45	2.03E-13	v46	2.68E-15
v47	6.92E-06	v48	3.79E-08	v49	3.05E-08	v50	2.26E-10	v51	1.59E-09
v52	2.56E-14	v53	4.03E-17	v54	5.42E-25	cr46	1.93E-20	cr47	5.74E-10
cr48	2.49E-04	cr49	3.79E-06	cr50	2.93E-05	cr51	4.42E-07	cr52	4.04E-06
cr53	8.24E-10	cr54	2.11E-11	cr55	1.33E-18	cr56	8.76E-22	mn48	2.02E-22
mn49	2.60E-14	mn50	1.50E-13	mn51	1.26E-05	mn52	4.00E-07	mn53	3.13E-06
mn54	1.02E-08	mn55	3.33E-09	mn56	1.03E-14	mn57	7.35E-18	fe51	2.41E-15
fe52	9.49E-04	fe53	7.98E-05	fe54	2.66E-03	fe55	9.41E-06	fe56	2.62E-05
fe57	2.74E-09	fe58	1.25E-10	fe59	3.11E-17	fe60	6.08E-20	co53	3.88E-18
co54	5.80E-14	co55	2.65E-04	co56	9.57E-06	co57	3.92E-06	co58	3.63E-09
co59	1.18E-09	co60	1.59E-14	co61	1.10E-16	co62	1.64E-23	ni55	5.96E-18
ni56	7.57E-02	ni57	4.17E-03	ni58	1.37E-02	ni59	2.12E-05	ni60	4.36E-06
ni61	6.88E-09	ni62	2.07E-08	ni63	1.17E-14	ni64	7.07E-17	ni65	2.07E-23
cu57	9.55E-13	cu58	8.59E-08	cu59	1.75E-04	cu60	1.21E-04	cu61	1.79E-05
cu62	2.03E-06	cu63	5.16E-08	cu64	6.46E-13	cu65	1.70E-14	cu66	2.45E-19
cu67	2.08E-23	zn59	1.06E-20	zn60	2.34E-03	zn61	2.09E-04	zn62	3.36E-03
zn63	1.14E-05	zn64	2.78E-07	zn65	4.05E-09	zn66	1.70E-10	zn67	1.25E-13
zn68	4.44E-16	zn69	2.65E-22	ga61	6.01E-18	ga62	2.11E-18	ga63	1.06E-06
ga64	2.41E-06	ga65	7.17E-07	ga66	1.58E-07	ga67	5.96E-09	ga68	2.72E-13
ga69	6.89E-14	ga70	3.53E-18	ga71	4.04E-21	ge63	4.48E-23	ge64	1.40E-05
ge65	2.62E-06	ge66	7.96E-05	ge67	6.62E-07	ge68	2.08E-07	ge69	1.97E-10
ge70	1.79E-12	ge71	5.32E-16	ge72	1.16E-18	ge73	1.25E-22		

© American Astronomical Society • Provided by the NASA Astrophysics Data System

1990ApJ...349..222T

TABLE 3

COMPOSITION AFTER DECAY OF RADIOACTIVE SPECIES

	$M/M_\odot$		$M/M_\odot$		$M/M_\odot$		$M/M_\odot$
d	3.40E-17 0	he3	1.46E-19 0	he4	2.10E+00 0	li6	5.10E-19 0
li7	4.50E-20 0	be9	7.64E-18 0	b10	2.73E-17 0	b11	6.47E-16 0
c12	1.14E-01 0	c13	4.46E-07 2	n14	2.71E-03 0	n15	4.40E-08 2
o16	1.48E+00 0	o17	3.73E-09 2	o18	8.68E-03 0	f19	8.63E-10 2
ne20	2.28E-01 0	ne21	3.02E-04 0	ne22	2.93E-02 0	na23	1.17E-03 0
mg24	1.47E-01 0	mg25	1.84E-02 0	mg26	1.71E-02 0	al27	1.59E-02 0
si28	8.43E-02 0	si29	9.70E-03 0	si30	7.30E-03 0	p31	1.13E-03 0
s32	2.49E-02 0	s33	1.15E-04 0	s34	1.11E-03 0	s36	2.51E-07 1
cl35	5.16E-05 0	cl37	6.24E-06 0	ar36	4.10E-03 0	ar38	3.08E-04 0
ar40	2.54E-09 1	k39	2.91E-05 1	k41	2.28E-06 1	ca40	3.31E-03 0
ca42	9.79E-06 1	ca43	2.81E-06 1	ca44	2.09E-04 1	ca46	3.78E-11 2
ca48	3.97E-17 2	sc45	1.89E-07 1	ti46	3.66E-06 2	ti47	7.00E-06 1
ti48	2.49E-04 0	ti49	3.82E-06 1	ti50	4.72E-11 2	v50	2.26E-10 0
v51	1.30E-05 1	cr50	2.93E-05 0	cr52	9.53E-04 0	cr53	8.30E-05 0
cr54	1.02E-08 1	mn55	2.75E-04 0	fe54	2.66E-03 0	fe56	7.57E-02 0
fe57	4.17E-03 0	fe58	3.75E-09 0	co59	1.96E-04 1	ni58	1.37E-02 0
ni60	2.46E-03 0	ni61	2.27E-04 0	ni62	3.36E-03 0	ni64	8.01E-13 2
cu63	1.25E-05 1	cu65	3.34E-06 2	zn64	1.67E-05 0	zn66	7.98E-05 0
zn67	6.68E-07 0	zn68	2.08E-07 1	ga69	1.97E-10 1	ga71	5.32E-16 0
ge70	1.79E-12 0	ge72	1.16E-18 1	ge73	1.25E-22 2		

When comparing our results to Woosley, Pinto, and Weaver (1988), we find that all of the latter nuclei show strong deviations, just for the reasons mentioned above (they performed postprocessing with a full network also for the phases of hydrostatic nucleosynthesis, therefore avoiding the problems discussed here). The only other large deviation occurs for ^{50}V, where we suspect proton captures during hydrostatic burning phases to be largely responsible for the abundance of this rare nucleus. Differences for the nuclei ^{1}H, ^{4}He, ^{13}C, ^{14,15}N, ^{17}O, and ^{19}F, representing either unburned fuel (^{1}H, ^{4}He) and (or) resulting from hydrogen burning, are easily explainable because we did not include the composition of the H envelope and also because ^{13}C, ^{15}N, ^{17}O, ^{19}F were not included in the hydrostatic network. There are other differences of a smaller but systematic nature, i.e., the nuclei from Ne through P show larger abundances in our calculation and S through Sc show smaller abundances. These differences are of the order of a factor of 2 and due to the structure and composition of the presupernova model. The origins of these differences and uncertainties entering the presupernova evolution will be discussed in Paper III (Hashimoto and Nomoto 1989).

b) Comparison to Abundance Observations in SN 1987A

A direct comparison between the calculated abundances and observations suffers from two complications. The ejecta were still not completely optically thin in all wavelengths at the time when the observations (discussed below) were taken, and therefore it is not certain if one sees the total mass of an element. Indications that the optically thin limit is attained come from an asymptotic constancy as a function of time, of observed line intensities. Other complications are given by the fact that only certain ionization stages are observed and assumptions about the temperature and density in the remnant are necessary for determining the total mass of a given element. Infrared observations at various times after explosion (Rank *et al.* 1989; Erickson *et al.* 1988; Danzinger *et al.* 1988; Aitken *et al.* 1988; Terndrup *et al.* 1988; Witteborn *et al.* 1989; Bregman *et al.* 1989) led to the following mass estimates in specific ionization stages (in units of $M_\odot$): Co, 0.0044 (280^d), 0.0028 (370^d), 0023 (400^d); Fe, 0.06 (280^d); Ni II, 2.6×10^{-3} (260^d), 3×10^{-3}(415^d); Ni I + II, 5×10^{-3} (415^d); Ar II 9×10^{-4} (415^d); Cl I, 7.4×10^{-4} (370^d); Ne II, 1.2×10^{-3} (370^d); O I, 0.2 (376^d); C I 6×10^{-3} (376^d). Recent results by Danziger *et al.* (1989) at 410^d give vaues for C(0.072), O(3.0), Si(0.102), Ar($>$0.0008), Ca($<$0.0105), Fe(0.098), Co(0.005), and Ni(0.0022). They are considered to be correct within a factor of 2–3.

The Co and Fe abundances are consistent with 0.07 $M_\odot$ of ^{56}Ni produced in the ejecta, which decays to ^{56}Co and finally ^{56}Fe and is required for the late exponential decline of the light curve (Shigeyama, Nomoto, and Hashimoto 1988; Woosley 1988; Arnett and Fu 1989). Ni isotopes or isotopes decaying into Ni with half-lives comparable to 260^d or longer are not existing in nature, therefore the quoted values of 2.6 and 3×10^{-3} in Ni II and 5×10^{-3} in total Ni should be due to stable Ni isotopes and can be regarded as constant in time within their uncertainties. The total amount of Ni predicted in our model is 1.97×10^{-2} $M_\odot$. Therefore, the present observations, assuming that they see all of the Ni mass, put a serious constraint on the stellar model. The dominant contributions to ^{58}Ni and also ^{61,62}Ni originate from the relatively neutron-rich zones inside 1.63 $M_\odot$ (see ^{58}Ni and ^{61,62}Zn in Fig. 6). A smaller Ni abundance requires that less matter from these mass zones should be ejected. Then the mass cut has (1) either to be moved further out (which can be achieved by employing a stronger shock energy—together with the ^{56}Ni constraint) or (2) the stellar model has to be altered.

The first possibility would be equivalent to a mass cut at 1.63 $M_\odot$, but would also reduce the amount of ^{56}Ni to 0.059 $M_\odot$ (the ejected masses after decay for this choice of the mass cut are given in Table 4; see also the discussion in § V and Fig. 12).

© American Astronomical Society • Provided by the NASA Astrophysics Data System

1990ApJ...349..222T

TABLE 4

COMPOSITION OF EJECTA FOR MASS CUT AT 1.63 $M_\odot$

	M/M$_\odot$		M/M$_\odot$		M/M$_\odot$		M/M$_\odot$
d	3.40E-17	he3	1.46E-19	he4	2.10E+00	li6	5.10E-19
li7	4.50E-20	be9	7.64E-18	b10	2.73E-17	b11	6.47E-16
c12	1.14E-01	c13	4.46E-07	n14	2.71E-03	n15	4.40E-08
o16	1.48E+00	o17	3.73E-09	o18	8.68E-03	f19	8.63E-10
ne20	2.28E-01	ne21	3.02E-04	ne22	2.93E-02	na23	1.17E-03
mg24	1.47E-01	mg25	1.84E-02	mg26	1.71E-02	al27	1.59E-02
si28	8.43E-02	si29	9.70E-03	si30	7.30E-03	p31	1.13E-03
s32	2.49E-02	s33	1.15E-04	s34	1.11E-03	s36	2.51E-07
cl35	5.04E-05	cl37	6.17E-06	ar36	4.09E-03	ar38	3.05E-04
ar40	2.46E-09	k39	2.19E-05	k41	1.50E-06	ca40	3.28E-03
ca42	8.36E-06	ca43	1.63E-06	ca44	1.09E-04	ca46	3.78E-11
ca48	3.97E-17	sc45	6.97E-08	ti46	3.35E-06	ti47	2.81E-06
ti48	1.55E-04	ti49	3.69E-06	ti50	4.72E-11	v50	2.26E-10
v51	9.01E-06	cr50	2.90E-05	cr52	8.36E-04	cr53	8.05E-05
cr54	1.02E-08	mn55	2.73E-04	fe54	2.66E-03	fe56	5.88E-02
fe57	2.41E-03	fe58	3.13E-09	co59	8.16E-05	ni58	3.84E-03
ni60	1.66E-03	ni61	1.05E-04	ni62	8.83E-04	ni64	8.60E-14
cu63	2.21E-06	cu65	1.10E-06	zn64	1.09E-05	zn66	1.96E-05
zn67	1.07E-07	zn68	2.87E-08	ga69	2.28E-11	ga71	5.45E-17
ge70	1.99E-13	ge72	1.12E-19	ge73	1.12E-23		

This is marginably compatible with the observational limits of $0.07 \pm 0.01\ M_\odot$. An increased explosion energy could improve the agreement, because it causes a stronger shock and produces a larger amount of ^{56}Ni, also at larger radii. The discussion in § VI, which includes the uncertainty of the supernova energy in an analytical approximation, results in a mass cut at $1.6 \pm 0.045\ M_\odot$, i.e., the error bar covers the number quoted above. A future paper will study the whole range of allowed supernova energies and its influence on the mass cut and ejected abundances with detailed numerical calculations. The second alternative would require a larger Y_e in the innermost ejected zones, which needs an alteration of the stellar model, in this case either a smaller size of the convective O-burning shell and (or) a smaller degree of mixing of Si shell-burning products into outer layers. In fact, the outer boundary of the convective layer may not be determined that accurately because of a rather flat entropy distribution there.

Ar is produced in our model with a total mass of 4.4×10^{-3} $M_\odot$. Again it would be useful to know the population of Ar I, in order to compare the total abundance. We predict a total Cl abundance of 5.78×10^{-5}. This is more than a factor of 10 smaller than observed. However, Cl is one of the elements affected by the reduced network for the hydrostatic burning phases. Arnett and Thielemann (1985) performed hydrostatic core He-burning with an extended network and also followed the weak *s*-process component in core He-burning of massive stars. It turned out that substantial amounts of ^{36}S and ^{37}Cl (and other intermediate mass nuclei) were produced by neutron captures of nuclei with $A > 20$. When generalizing their results for a 6 $M_\odot$ He core, we expect about 3×10^{-4} $M_\odot$ of ^{37}Cl, which is in agreement within a factor of 2 of the observed value for Cl I. The lower limit for Si corresponds to 30% of our predicted value (0.1).

The early observed values of Ne, O, and C are much below our predictions. We assume in agreement with Terndrup *et al.* (1988) that they represented only part of the total mass in the ejecta. However, the late observations provide a lower limit for C which comes closer to the predicted value of 0.114 (32%). Preliminary findings by Phillips (1988) that in total 1–2 $M_\odot$ of O are observed in the ejecta are also comparable to the recent results by Danziger *et al.* (1989), who determined oxygen values of 3.0 $M_\odot$. Dependent on the assumed temperatures the value is claimed to be correct within a factor of 2–3, which covers our prediction of $\approx 1.5\ M_\odot$. If these measurements can be further refined, they might contribute significantly to an indirect determination of the experimentally uncertain ^{12}C(α, γ)^{16}O rate. The 18 $M_\odot$ model of Woosley, Pinto, and Weaver (1988), which was calculated with two rates (Caughlan and Fowler 1988; Caughlan *et al.* 1985) which probably represent the lower and the upper limit within the present uncertainties (Filippone, Humblet, and Langanke 1989), predicts 0.2 and 0.5 $M_\odot$ of ^{16}O, respectively. This would mean that probably stellar models with $M < 20\ M_\odot$ can be excluded as progenitors of SN 1987A and that the higher value of the ^{12}C(α, γ) rate should be preferred. A final judgement has to wait, however, for a more detailed evaluation of the observed O mass.

c) *Long-lived Radioactivities*

Besides ^{56}Ni there are a number of radioactive nuclei which will decay on time scales of ms to 10^7 yr. Their detailed abundances can be obtained from Table 2. Here we want to concentrate on only a few nuclei which, by a combination of their abundances and half-lives, can be of importance. These nuclei are ^{56}Co, ^{57}Co, ^{55}Fe, ^{44}Ti, and ^{22}Na with total masses of $0.075, 4.17 \times 10^{-3}, 2.65 \times 10^{-4}, 2.09 \times 10^{-4}$, and 1.01×10^{-7} $M_\odot$, according to Table 2. For a compromise between the different choices of mass cuts, discussed above, we use here the masses associated with a 1.6 $M_\odot$ mass cut, i.e., 0.07, 3.23×10^{-3}, 2.59×10^{-4}, 1.23×10^{-4}, and 1.01×10^{-7} $M_\odot$. Generally, with the exception of ^{55}Fe, the daughter nucleus—

© American Astronomical Society • Provided by the NASA Astrophysics Data System

1990ApJ...349..222T

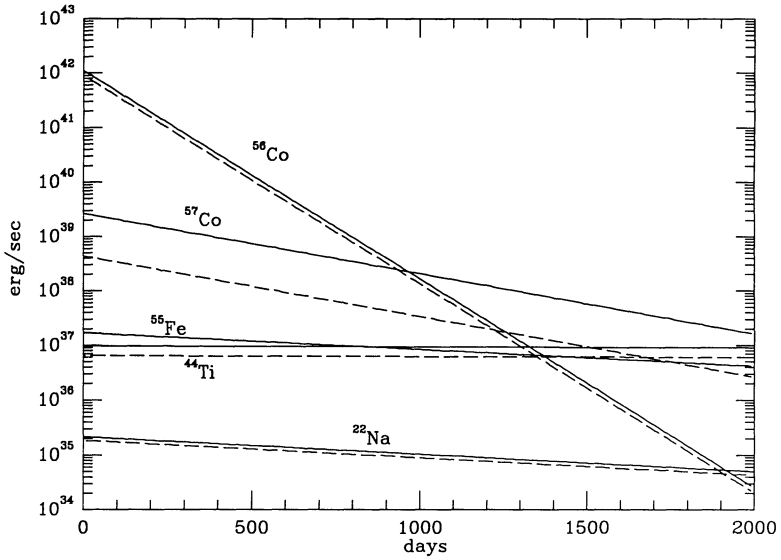

FIG. 9.—Energy generation as a function of time after the supernova explosion, due to decay of long-lived radioactive nuclei. Solid lines include the total atomic Q-value; dashed lines exclude the energy in neutrinos, which will escape without energy deposition. The decay energy of ^{55}Fe is only contained in neutrinos. Except for very early times, the bolometric light curve is identical with the curve labeled ^{56}Co until 200–300 days, when the leakage of X-rays and gamma-rays becomes important.

after beta-decay or electron capture—is produced in an excited state. The ground state is reached by one or several gamma transitions, which might be observed with gamma-ray detectors on balloons or satellites (especially *GRO* with its increased sensitivity). Photons, positron-electron annihilations after β^+-decays, and the kinetic energy given to the decay products can contribute to the light curve at later times.

The number of photons released for each of the transitions, occurring in the daughter nucleus after beta-decay, is equal to the number of decays N_d, multiplied with the appropriate percentage of the specific transition. The total energy released corresponds to the product of the number of decays with the decay Q-value. This is expressed in the following equations:

$$N_d(t) = -\dot{N}(t) = \lambda N_0 \exp(-\lambda t) \quad (3)$$

$$\dot{E}(t) = Q N_d(t) = Q\lambda N_0 \exp(-\lambda t), \quad (4)$$

where $\lambda = \ln 2/t_{1/2}$ is the decay rate of the nucleus. The initial number of radioactive nuclei can be calculated from their total mass by $N_0 = M/Am_u$ with A being the nucleon number of the nucleus; m_u; the atomic mass unit; and M, the mass from Table 1. When using the half-lives of 78^d.76, 271^d.3, 2.7 yr, 54.2 yr, and 2.602 yr, and atomic Q-values of 4.566, 0.835, 0.232, 3.919, and 2.842 MeV, we obtain the energy generation rates in ergs s^{-1} and the total number of decays per second as shown in Figures 9 and 10. The Q-value used for ^{44}Ti combines the subsequent decays of ^{44}Ti and ^{44}Sc. These Q-values contain the kinetic energy of the decay products, the energy in photons, the annihilation energy of positron-electron paris in β^+-decays, and the neutrino energy. At densities prevailing in the expanding remnant, neutrinos will escape freely and their energy has to be subtracted, which leaves corrected values for the appropriate energy release of 3.695, 0.136, 0.0, 2.966, and 2.444 MeV (Lederer and Shirley 1978; Woosley, Pinto, and Hartmann 1989), resulting in the dashed lines in Figure 9. Because the electron capture on ^{55}Fe leads only to an energetic neutrino, there is no dashed line for ^{55}Fe displayed in Figure 9. The gamma transitions for the other decays are the following (rounded to full percent values): ^{56}Co, 847 keV (100%), 1038 keV (14%), 1238 keV (68%), 1772 keV (16%), 2599 keV (17%); ^{57}Co, 122 keV (86%), 136 keV (11%); ^{44}Ti, 78 keV (93%), 68 keV (88%), 147 keV (9%), 1157 keV (100%); ^{22}Na, 1275 keV (100%). If positrons from β^+-decay annihilate with electrons, the full Q-value deduced from atomic masses, but corrected for neutrino losses, becomes available and the resulting high energy photons as well as the ones from gamma transitions, are Compton-scattered and completely thermalized. Then the sum of the dashed lines in Figure 9 corresponds to the bolometric light curve of the supernova. Escaping high-energy photons or positrons at lower densities (and later times) will lead to a reduction of the light curve in comparison to these functions, as it has been observed after days 200–300 (see also Fu and Arnett 1989; Kumagai *et al.* 1989; Woosley, Pinto, and Hartmann 1989). From the display it can be seen clearly, that the light curve will be dominated as a function of time first by the decay of ^{56}Co, and then ^{57}Co and ^{44}Ti, if we neglect possible radiation from a pulsar. ^{22}Na never plays a dominant role for the light curve. At late times, when the high energy photons escape freely, Figure 10 can be used to calculate the photon flux (per cm^2 and second) by multiplying with 3.34×10^{-48} (distance Earth–LMC = 50 kpc) and the appropriate percentage of the individual gamma-transitions, given above. A mass cut at 1.63 rather than 1.6 $M_\odot$would reduce the lines for ^{57}Co and ^{44}Ti in Figures 9 and 10 to about 70% of their value.

V. SUPERNOVA NUCLEOSYNTHESIS AND CHEMICAL EVOLUTION

a) Comparison with Solar Abundances

It has been customary to compare abundances of explosive nucleosynthesis events to solar abundances. We display such a comparison in Figure 11 (for a mass cut at 1.6 $M_\odot$). It does not necessarily make sense when one wants to explain the (non solar) abundances in the LMC. Even in our Galaxy such a comparison is only meaningful, when nucleosynthesis results are integrated over the total mass range of type II supernovae and also over the Galactic age. Woosley and Weaver (1986)

© American Astronomical Society • Provided by the NASA Astrophysics Data System

1990ApJ...349..222T

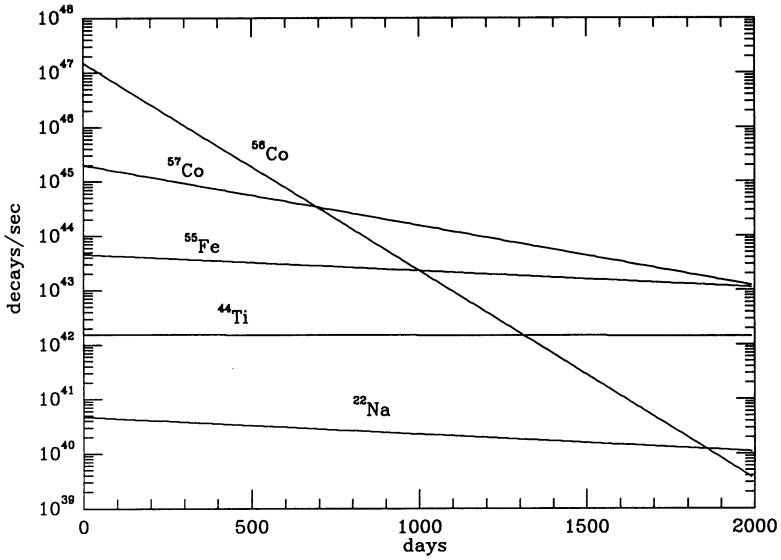

FIG. 10.—Decays per second of long-lived radioactive nuclei. With the exception of ^{55}Fe, the decays lead to gamma transitions: ^{56}Co, 847 keV (100%), 1038 keV (14%), 1238 keV (68%), 1772 keV (16%), 2559 keV (17%); ^{57}Co, 122 keV (86%), 136 keV (11%); ^{44}Ti, 78 keV (93%), 68 keV (88%), 147 keV (9%), 1157 keV (100%); ^{22}Na, 1275 keV (100%). If the photons escape freely (i.e., at late times), the photon flux at Earth in photons cm^{-2} and s^{-1} (50 kpc) can be obtained by multiplying the decay curves with the percentages for the individual transitions and 3.34×10^{-48}.

find, however, that when weighting the ejected mass of heavy element in Type II supernovae with the present initial mass function, the average supernova of importance for heavy element nucleosynthesis lies in the range of 20–30 $M_\odot$. Supernovae in this mass range should therefore be most responsible for the abundance distribution in our Galaxy (although not each of them will produce average abundances).

The ratios in Figure 11 are normalized to ^{28}Si, which has an overproduction factor over solar of 25.2 within the 6 $M_\odot$ He core. This translates into a factor of about 7.6 for the entire 20 $M_\odot$ star. Nuclei heavier than Si and P are on average produced by a factor of 2–4 less than ^{28}Si. This is similar to the results obtained by Woosley, Pinto, and Weaver (1988) for their 18 $M_\odot$ star. ^{28}Si, while also produced in explosive O-burning, has large contributions from the zones of hydrostatic neon burning (60%), which are unaltered during the explosion (see Figs. 3 and 2). Essentially all heavier elements originate from explosive processing. Thus the ratio between elements heavier than Si and P to lighter elements reflects mainly the size of hydrostatic zones to the explosively processed ones and is a function of stellar mass (and perhaps the methods used in stellar evolution calculations). The abundances of elements lighter than Si and P, i.e., C, O, Ne, Ma, Mg, and Al originate from hydrostatic burning phases in stellar evolution. The products of C- and Ne-burning have large abundances. The reason is the existence of an extended shell of combined C and Ne-burning, ranging from 1.8 to 3.7 $M_\odot$ in the progenitor star (see. Fig. 10 in Nomoto and Hashimoto 1988). This is different from the results of Woosley, Pinto, and Weaver (1988) and the reason that in their case the carbon- and neon-burning products ^{20}Ne, ^{23}Na, and ^{24}Mg are not at the same level of overabundance as ^{16}O and ^{28}Si. This zone contains large quantities of ^{20}Ne and ^{24}Mg. Ne-burning destroys the C-burning product ^{23}Na and produces a variety of other nuclei like ^{25}Mg, ^{27}Al, ^{29,30}Si, and ^{31}P (Thielemann and Arnett 1985). Such a behavior is reflected in Figure 4.

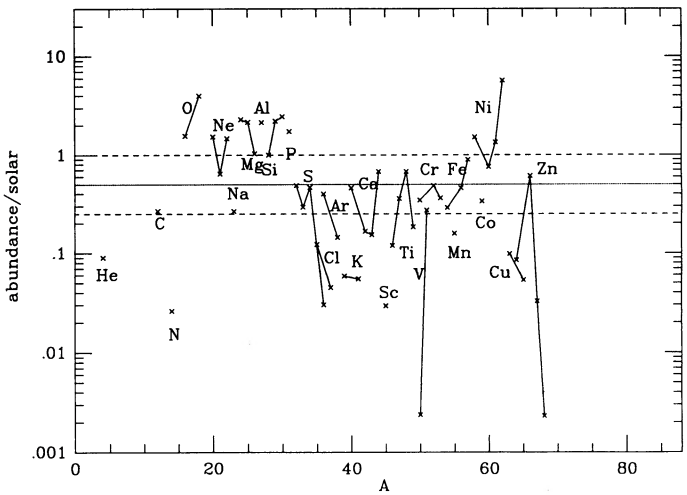

FIG. 11.—Composition of the supernova ejecta in comparison to solar abundances (normalized to ^{28}Si). Only elements inside the 6 $M_\odot$ He core are considered. Isotopes of each element are connected by lines. All elements lighter than P are dominated by nucleosynthesis during hydrostatic stellar evolution. Elements from S to Ni, which originate from explosive processing, show similar ratios within a factor of 2 or 3. The overabundances of ^{58,61,62}Ni are strongly dependent on the position of the mass cut and come from regions with small Y_e.

The ratio of ^{12}C to ^{16}O is closely linked to the "effective" ^{12}C(α, γ)^{16}O rate during core He-burning. This effective rate is determined by three factors: (1) the actual nuclear rate which is recently in doubt again (Kremer *et al.* 1988; Filippone, Humblet, and Langanke 1989; Caughlan *et al.* 1985; Caughlan and Fowler 1988); (2) the amount of semiconvection and overshooting, mixing fresh He fuel into the core at late phases of He-burning, when the temperatures are relatively high and favor alpha-capture on ^{12}C; and (3) the stellar mass which determines the central temperature during He-burning. The features seen in Figure 11 demonstrate that the star experienced a large ^{12}C(α, γ) rate as a result of all three effects.

The products of explosive burning from S to Cu originate

© American Astronomical Society • Provided by the NASA Astrophysics Data System

1990ApJ...349..222T

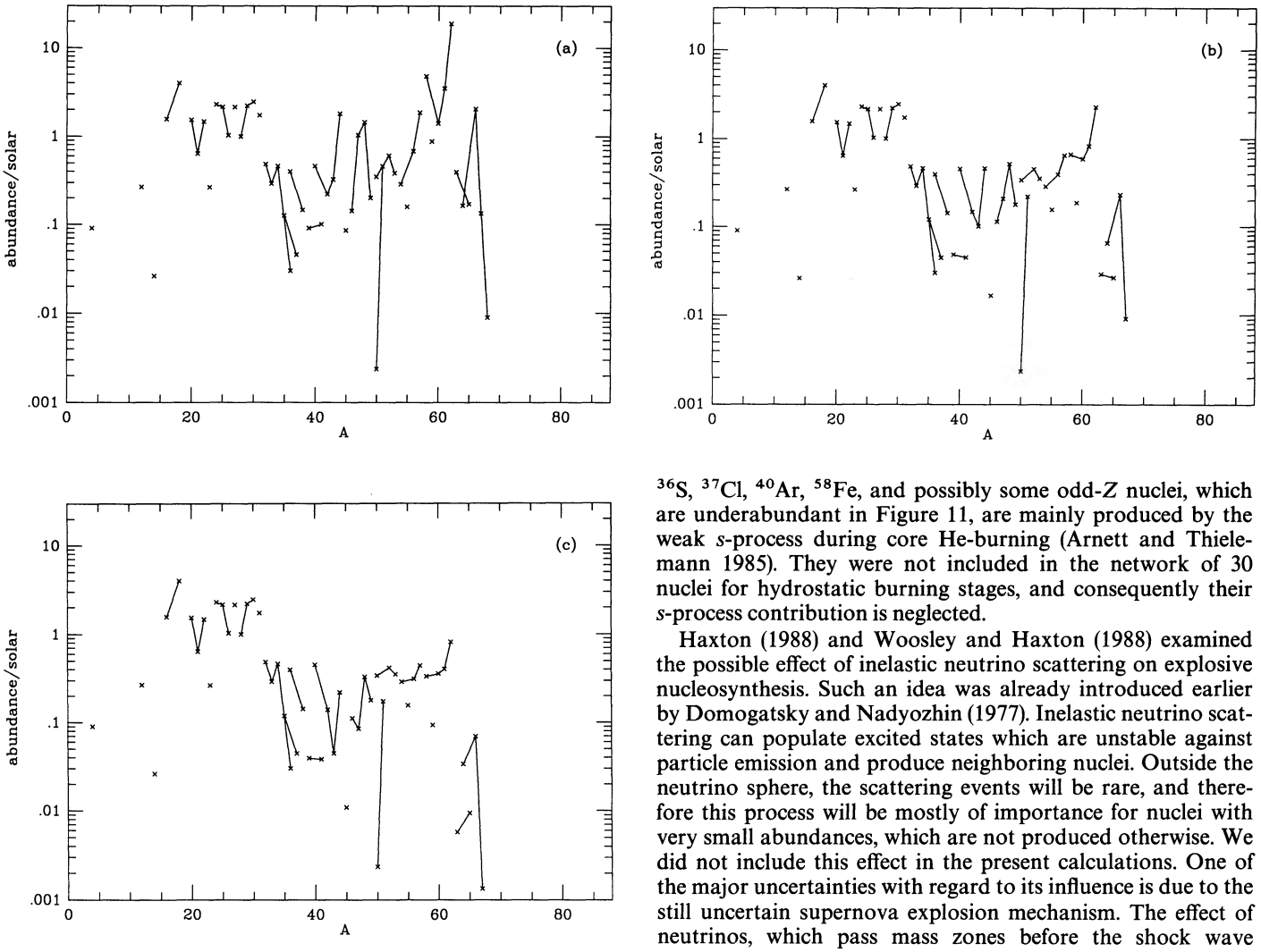

FIG. 12.—The same as Fig. 11 for three different values of the mass cut: (*a*) 1.53, (*b*) 1.63, and (*c*) 1.65 $M_\odot$. This corresponds to 0.102, 0.0059, and 0.047 $M_\odot$ of ejected ^{56}Ni. Prominent differences can be seen for nuclei which originate from an alpha-rich freeze-out or mass zones with a larger neutron excess ($M < 1.63\ M_\odot$). This is reflected in nuclei like ^{44}Ca(^{44}Ti), ^{48}Ti(^{48}Cr), ^{57}Fe(^{57}Ni), ^{58}Ni, ^{61}Ni(^{61}Zn) and ^{62}Ni(^{62}Zn). The stable Ni isotopes seem to show the largest changes. Fig. 12*b* corresponds to the Ni abundances from IR observations. The observed Ni/Fe ratio and the amount of radioactive ^{56}Ni in SN 1987A will determine uniquely the mass cut and the explosion energy.

mainly from mass zones up to 1.8 $M_\odot$. They fall well along a line of constant overproduction (within reasonable errors). The nuclei ^{58,61,62}Ni which show large overabundances are produced in form of the neutron-rich species ^{58}Ni and ^{61,62}Zn. Their production is strongly dependent on Y_e and varies therefore with the position of the mass cut between ejected matter and the remaining neutron star (see Fig. 12 for choices of 1.53 $M_\odot$, 1.63 $M_\odot$, and 1.65 $M_\odot$ and the discussion § IV*b*). Especially for the Ni abundances, the position of the mass cut is crucial and one would expect lower mass Type II supernovae to eject more of these neutron-rich species. For a general discussion of the composition of hydrostatic neutron-rich Si-burning, see also Thielemann and Arnett (1985). This could explain the observed very high Ni abundances in some supernova remnant like the Crab (Henry and Fesen 1988), if they are not explained away by atomic or other effects. A few nuclei like ^{36}S, ^{37}Cl, ^{40}Ar, ^{58}Fe, and possibly some odd-Z nuclei, which are underabundant in Figure 11, are mainly produced by the weak *s*-process during core He-burning (Arnett and Thielemann 1985). They were not included in the network of 30 nuclei for hydrostatic burning stages, and consequently their *s*-process contribution is neglected.

Haxton (1988) and Woosley and Haxton (1988) examined the possible effect of inelastic neutrino scattering on explosive nucleosynthesis. Such an idea was already introduced earlier by Domogatsky and Nadyozhin (1977). Inelastic neutrino scattering can populate excited states which are unstable against particle emission and produce neighboring nuclei. Outside the neutrino sphere, the scattering events will be rare, and therefore this process will be mostly of importance for nuclei with very small abundances, which are not produced otherwise. We did not include this effect in the present calculations. One of the major uncertainties with regard to its influence is due to the still uncertain supernova explosion mechanism. The effect of neutrinos, which pass mass zones before the shock wave arrives, will be wiped out by explosive processing in the shock wave. Therefore, only neutrino scattering after explosive processing will be of importance. Then the neutrino flux will depend strongly on the time elapsed since the core collapse, which can be 30 ms for a prompt shock or 1 s for the delayed mechanism, which will already lead to a substantial reduction of the neutrino flux. Thus the importance is not yet completely forseeable. The final answer is coupled to the solution of the supernova problem and the detailed evaluation of the cross sections for neutrino induced particle emission for all nuclei in the network.

b) Chemical Evolution of Galaxies

In stellar abundance determination and chemical evolution calculations of galaxies it is customary to use the quantity $[X/Fe] = \log [(X/Fe)/(X/Fe)_\odot]$. In Table 5 we compare the predictions for this 20 $M_\odot$ star to the average observed value for low-metallicity stars in the solar neighborhood with $[Fe/H] < -1$, which should represent an average value for Type II supernovae ejecta (see discussion below). The two columns represent the results for mass cuts between neutron star and ejecta at 1.59 $M_\odot$ and 1.63 $M_\odot$ and correspond to the abundances in Table 3 and 4. The observational values come from Carbon *et al.* (1987), Tomkin and Lambert (1984), Tomkin, Sneden, and Lambert (1986), Gratton and Sneden (1987), Luck

© American Astronomical Society • Provided by the NASA Astrophysics Data System

1990ApJ...349..222T

TABLE 5

COMPARISON WITH ABUNDANCE RATIOS OF LOW-METALLICITY STARS

Ratio	$M_c = 1.59\ M_\odot$	$M_c = 1.63\ M_\odot$	Observed for [Fe/H] < −1
[C/Fe]	−0.29	−0.18	0.0
[O/Fe]	0.49	0.60	0.5
[Mg/Fe]	0.62	0.73	0.4
[Si/Fe]	0.34	0.45	0.4
[S/Fe]	0.00	0.11	0.5
[Ca/Fe]	−0.07	0.03	0.3
[Ti/Fe]	0.14	0.05	0.2
[Cr/Fe]	−0.01	0.05	0.1
[Ni/Fe]	0.63	0.26	0.3

and Bond (1985), Hartmann and Gehren (1988), Magain (1987), and Francois (1986, 1988) and are nicely collected in a compilation by Gehren (1988) and also Wheeler, Sneden, and Truran (1989). The observational data show a scatter of 0.1–0.2. Before discussing the comparison between both sets of data, one should somewhat discuss their logical connection.

We start Galactic chemical evolution at point $t = 0$ with a set of freshly born stars whose number as a function of stellar mass follows an initial mass function. The first events which contribute to heavy metal pollution will be the most massive Type II supernovae, due to their short lifetime, followed by less massive Type II supernovae and finally intermediate-mass stars (IMS; $1 < M/M_\odot < 9$), which do not undergo explosive events but contribute via mass loss and planetary nebula ejection, before turning into white dwarfs. For a given initial mass function, the rate of metal enhancement [Fe/H] as a function of time depends on the star formation rate. For reasonable choices within the solar neighborhood, Matteucci (1987), Matteucci and François (1989), and Mathews, Bazan, and Cowan (1990) find that the dividing line between Type II supernovae and intermediate-mass stars is located between [Fe/H] = −3 and −2. This does not mean that only IMSs will contribute for [Fe/H] > −2, massive stars will continue to form, evolve fast, and eject their debris into the interstellar medium, but IMSs will contribute at that metallicity for the first time. Type Ia supernovae have a more complicated origin. They are explained as exploding white dwarfs, which undergo central carbon ignition under degenerate conditions and total disruption (Nomoto, Thielemann, and Yokoi 1984; Woosley, Axelrod, and Weaver 1984; Thielemann, Nomoto, and Yokoi 1986). Among the possible scenarios, this ignition will take place when the more massive partner in a binary CO white dwarf system exceeds the Chandrasekhar mass due to CO accretion via Roche-lobe overflow (Iben and Tutukov 1984, 1985). The time scale for such an event is given by the evolution times scales of two 5–9 $M_\odot$ mass stars in a binary system, including the phases of common envelope evolution and gravitational radiation during the binary white dwarf phase, for getting close enough to initiate Roche-lobe overflow. The shortest evolution time scale for a close system of massive IMSs is a few times 10^7–10^8 yr. In a simple chemical evolution model, that corresponds to [Fe/H] ≈ -1.

Except for C, none of the elements listed in Table 5 have strong contributions from IMSs. Fe group nuclei are the main burning product of Type I supernovae, with smaller contributions to Si–Ca. Type II supernovae are expected to produce some Fe and large amounts of O through Ca. Therefore, we only have to explore the influence of Type I and Type II supernovae on the time or metallicity [Fe/H] evolution of O/Fe through Ni/Fe. In O/Fe Mg/Fe, Si/Fe, S/Fe, and Ca/Fe, one sees a relatively constant ratio for low-metallicity stars for [Fe/H] from −2.5 to −1, with the values quoted in the third column of Table 5. Then follows a decline to [X/Fe] = 0 at [Fe/H] = 0. Such a behavior is entirely explainable by the dominant contribution of Type II supernova to O through Ca. The decline from the average value for Type II supernovae to O is due to the large production of Fe in Type I supernovae for later times ([Fe/H] > −1). Thus, we have a clear indication from observations that type II supernovae do *not* produce the entire amount of Galactic Fe. This is only true within a factor of 2–3, i.e., 0.3–0.5 dex, while the remaining part has to come from Type I supernovae (see also the discussion in Arnett, Schramm, and Truran 1989). The remaining open question is why the observed values of all ratios [X/Fe] seem to be constant from [Fe/H] = −2.5 to −1. This can be understood when we notice that the first contribution by a 30 $M_\odot$ star will be at −3.9, for a 12 $M_\odot$ star this point is at −3, and the lowest mass Type II supernova will contribute for the first time between −3 and −2. At each point in the evolution (t or [Fe/H]) we see the integrated contribution of all stars from $M_{\rm low}(t)$ to the upper mass limit of Type II supernovae $M_{\rm up}$. With $M_{\rm low}$ being equal to the lower mass limit of Type II supernovae for [Fe/H] somewhere between −3 and −2, we will find an averaged contribution over the entire mass range of Type II supernovae for all larger metallicities, which is reflected in the constant ratios. With future observations, which hopefully will be able to obtain measurements down to [Fe/H] = −4.5 (Beers, Preston, and Schectman 1990), we should be able to identify individual signatures of supernovae from a changing mass range $M_{\rm low}(t)$ to $M_{\rm up}$.

It is therefore not hard to understand that an individual supernova, like SN 1987A, cannot explain the average values listed in Table 5. However, one can notice that O through Si behave close to the observed values. It is expected that more massive Type II supernovae show an overproduction of S through Ca which is comparable to O through Si. This can be deduced from the calculation for a 25 $M_\odot$ star by Woosley and Weaver (1986) or the calculation by Woosley, Pinto, and Weaver (1988) for a 20 $M_\odot$ star which still included an enhanced treatment of overshooting and therefore behaves like a more massive star. It is also expected that less massive supernovae contribute larger amounts of C (lower temperatures for He-burning) and lead to an average of [C/Fe] = 0. The values given in brackets, which correspond to a slightly different mass cut at 1.63 $M_\odot$ show that none of the ratios depends strongly on this choice, except for [Ni/Fe]. This might give an indication that, dependent on the progenitor mass and the details of the explosion mechanism, one can expect widely varying values in different supernovae remnants.

For the future improvement of chemical evolution calculations, it is essential that explosive nucleosynthesis calculations become available for the whole mass range of Type II supernovae. This might finally lead to an astronomical determination of the $^{12}C(\alpha, \gamma)$ rate. In this respect it is interesting that the calculations by Matteucci (1987) led to an enhanced [C/Fe] ratio for the metallicity range [Fe/H] > −2 by the contribution from intermediate mass stars. Their yields were based on stellar evolution calculations by Renzini and Voli (1981) and the rate by Fowler, Caughlan, and Zimmerman (1975) which is about a factor of 2 smaller than the rate by

© American Astronomical Society • Provided by the NASA Astrophysics Data System

1990ApJ...349..222T

Caughlan *et al.* (1985) and close to the recently recommended value by Caughlan and Fowler (1988). This might be an indications that the 1975 and 1988 values are too small, and the truth is probably closer to the 1985 value or in between.

VI. THE NEUTRON STAR MASS

Without a self-consistent explosion calculation and with an artificially induced shock wave, there is no way to predict the correct mass cut between the ejecta and the neutron star remnant. However, the amount of ^{56}Ni deduced from the late light curve can be used as a constraint. When ejecting the total material in the Si zone, which underwent core or shell O-burning during the precollapse evolution and explosive Si-burning during the supernovae explosion, a total amount of 0.14 $M_\odot$ of ^{56}Ni would come with it. This is in contradiction to the observed value of 0.07 ± 0.01 $M_\odot$. In order to obtain this value, a mass cut at 1.6 ± 0.025 $M_\odot$ is required in the given stellar model. In a prompt explosion the shock would originate further inside the star and produce a larger amount of Ni. The Ni inside 1.6 $M_\odot$ would be required to fall back. This Ni would undergo electron captures and photodisintegrations in the neutron star on short time scales and not contribute to the decay heat, observable in the late-time light curve. In case of a delayed explosion, early calculations by Wilson *et al.* (1986) showed that the Fe core grows due to accretion by 0.2 to 0.3 $M_\odot$ for a 25 $M_\odot$ star before the shock is revived, which was almost the entire Si shell in that calculation. In our case, the Fe core mass is 1.4 $M_\odot$ and a mass cut at 1.6 $M_\odot$ would therefore be a natural choice. For both scenarios (prompt and delayed explosions), our assumption would still be valid that the ejecta consist of material which was essentially unaltered between the onset of the collapse and the passage of the shock wave.

The proto–neutron star with a baryonic mass of 1.6 ± 0.025 $M_\odot$ will release a binding energy of about 3×10^{53} ergs in blackbody radiation of neutrinos during its contraction to neutron star densities, which has been observed with the Kamiokande II and IMB detectors (Hirata *et al.* 1987; Bionta *et al.* 1987). The gravitational mass is then given by

$$M_g = M_b - E_{\rm bin}/c^2 \,. \tag{5}$$

For reasonable uncertainties in the equation of state, Lattimer and Yahil (1989) obtained a relation between gravitational mass and binding energy:

$$E_{\rm bin} = (1.5 \pm 0.15)\left(\frac{M_g}{M_\odot}\right)^2 \times 10^{53} \text{ ergs} \tag{6}$$

$$E_{\rm bin} = (0.0839 \pm 0.0084)\left(\frac{M_g}{M_\odot}\right)^2 M_\odot\, c^2 \,. \tag{7}$$

Applying equations (6) and (7) results in a gravitational mass of the formed neutron star of $M_g = 1.43 \pm 0.03$ $M_\odot$. This number does not include the uncertainties in the observed values of the explosion energy. While calculations are underway for a minimum and maximum value of $E_{\rm SN}$ with the main focus on the effect on nucleosynthesis products, we want to use a few simple analytic arguments here, in order to estimate the resulting uncertainty in the neutron star mass. In § II*b*, we used the fact that in a radiation-dominated bubble behind the shock front, temperatures beyond 5×10^9 K, which characterize complete Si-burning and result in ^{56}Ni as dominant abundance, were obtained within a radius of 3500 km for an explosion energy of 10^{51} ergs. This radius varies with the explosion energy as $E_{\rm SN}^{1/3}$ and therefore corresponds to 4090 km and 3110 km for the maximum (1.6×10^{51} ergs) and minimum (0.7×10^{51} ergs) energy. In the 20 $M_\odot$ model, this gives an uncertainty in mass of ± 0.02 $M_\odot$. When one moves the outer boundary of the zone in which ^{56}Ni is the dominant burning product, the inner mass cut between ejecta and the neutron star has to be moved accordingly, due to the constraint on the total amount of ejected ^{56}Ni. Thus the combined uncertainty, including the possible errors in explosion energy and ^{56}Ni abundance, gives a baryonic mass of the neutron star of 1.6 ± 0.045 $M_\odot$. This mass is also consistent with the value quoted in §§ IV*b* and V*a*; in order to avoid excessive abundances of stable Ni. Employing again equations (6) and (7), we obtain the result

$$M_b = 1.6 \pm 0.045\ M_\odot \,, \tag{8}$$

$$M_g = 1.43 \pm 0.05\ M_\odot \,, \tag{9}$$

which is in close agreement with observed neutron star masses. It is also in agreement with the limits inferred from the neutrino pulse, $M_g = 1.3$–1.5 $M_\odot$, $M_b < 1.7$ $M_\odot$ (Burrows 1988). Such an analysis was possible for the first time because the mass of ^{56}Ni could be identified in SN 1987A. It does, however, not include possible uncertainties of the stellar model.

The remaining question is how much uncertainties in the stellar evolution model and the allowed mass range for SN 1987A (19 ± 3 $M_\odot$) could affect the result. A 16 $M_\odot$ star would produce a smaller neutron star than the 20 $M_\odot$ model used in the present calculation. On the other hand, models with $M < 20$ $M_\odot$ cannot produce enough ^{16}O to account for the observed abundances. The 18 $M_\odot$ models of Woosley, Pinto, and Weaver (1988) give values only in the range for 0.24 to 0.4 $M_\odot$, depending on the ^{12}C(α, γ) rate. Given the constraint that the mass of ejected oxygen is larger than that (Phillips 1988; Danziger *al.* 1989), we have to exclude models with $M < 20$ $M_\odot$ and the lower limits of equations (8) and (9) present the lower bound of the neutron star mass. We deduce the upper bound from the following discussion. As outlined in § III*a*, the neutron star mass is approximately $M_{\rm NSE} - M_{\rm NI}$, where $M_{\rm NSE}$ denotes the mass included within a 3500 km radius and $M_{\rm Ni}$ the ejected mass of ^{56}Ni (0.07 ± 0.01 $M_\odot$) with some other neutron-rich iron-peak elements. $M_{\rm NSE}$ depends on the presupernova density structure, which is most influenced by the location of the burning shell of carbon and oxygen. (The uncertainty of the Fe core mass due to mixing in the silicon burning shell is much less important for $M_{\rm NSE}$.) For stars as massive as 20 $M_\odot$, a larger ^{12}C(α, γ) rate and a larger amount of overshooting mixing at the edge of the convection zone would lead to a larger $M_{\rm NSE}$ because of the smaller ^{12}C abundance and the weaker C shell burning (Nomoto and Hashimoto 1988; Woosley and Weaver 1988). The 6 $M_\odot$ He core model adopted in the present study assumes no overshooting (Nomoto and Hashimoto 1988), while model 20B by Woosley and Weaver (1988) includes overshooting, and both models assume the large 1985 ^{12}C(α, γ) rate. The explosive nucleosynthesis calculation for model 20B with $E_{\rm SN} = 1.2 \times 10^{51}$ ergs (Woosley, Pinto, and Weaver 1988) gives an upper limit for $M_{\rm NSE}$ which is approximately 1.73 $M_\odot$ (0.16 $M_\odot$ of iron peak elements in the ejecta plus 1.57 $M_\odot$ in the core with their choice of a mass cut). By taking into account the uncertainties of $E_{\rm SN}$, the upper limit to the baryonic mass of the neutron star would then be $M_b \approx$ 1.7 $M_\odot$. This upper limit is somewhat "soft" as we do not have

© American Astronomical Society • Provided by the NASA Astrophysics Data System

1990ApJ...349..222T

comparable information for a 22 $M_\odot$ star. Such a value is, however, consistent with the one inferred from the neutrino observations (1.7 $M_\odot$; Burrows 1988). This upper limit is important with respect to the recent (but yet to be confirmed) observation of a pulsar in SN 1987A with frequency of $\nu = 1.968$ kHz (Kristian *et al.* 1989). Friedman, Ipser, and Parker (1986) find maximum frequencies of an $M_b = 1.4\ M_\odot$ uniformly rotating neutron star, before it becomes unstable against $m = 3$ and 4 modes, to be 1.58 kHz (very soft equation of state [EOS]; Canuto and Chitre 1974), 0.92 kHz (Bethe and Johnson 1974; intermediate), and 0.61 kHz (Pandharipande and Smith 1975; stiff). Thus, an $M_b = 1.4\ M_\odot$ neutron star could not withstand such rotation frequencies, even for the softest EOS. In order to be stable at frequencies around 2 kHz higher masses are required which depend on the EOS: $\nu = 2.06$ kHz, $M_g = 1.49\ M_\odot$, $M_b = 1.68\ M_\odot$, $M_{g,\max}(\nu = 0) = 1.36\ M_\odot$ (Canuto and Chitre 1974; very soft); $\nu = 1.98$ kHz, $M_g = 1.66\ M_\odot$, $M_b = 1.87\ M_\odot$, $M_{g,\max}(\nu = 0) = 1.46\ M_\odot$ (Arponen 1972; soft); $\nu = 1.82$ kHz, $M_g = 2.14\ M_\odot$, $M_b = 2.44\ M_\odot$, $M_{g,\max}(\nu = 0) = 1.85\ M_\odot$ (Bethe and Johnson 1974; intermediate). This means that with our upper limit of $M_b = 1.7\ M_\odot$, $M_g < 1.52\ M_\odot$ from equation (7), only the softest EOS and slightly less soft EOSs would be allowed. In that respect, this observation (if it will be confirmed) would be of utmost importance to nuclear physics, putting severe constraints to the neutron star EOS.

When taking into account that most recent mass determination of the binary pulsar ($M_g = 1.442 \pm 0.003\ M_\odot$; Taylor and Weisberg 1989) excludes the softest EOS (Canuto and Chitre 1974), because it allows only for a maximum gravitational mass for zero rotation of $M_g = 1.36\ M_\odot$; then only a very narrow margin is left for the neutron star EOS (see Friedman, Ipser, and Parker 1989 for similar conclusions). Larger neutron star masses than mentioned here could be explained by accretion after the explosion (Woosley and Chevalier 1989). But such an effect would only be of interest for the present discussion when the accreted matter is completely mixed. Otherwise the matter would consist mostly of the innermost part of the initial ejecta, i.e., ^{56}Ni, and the ^{56}Ni constraint would still be valid and limit the mass to the previously discussed values.

VII. SUMMARY

The 20 $M_\odot$ model (6 $M_\odot$ He core) by Nomoto and Hashimoto (1988) was utilized to perform explosive nucleosynthesis calculations for SN 1987A with an explosion energy of 10^{51} ergs. Explosive processing happens predominantly only within the inner 2.0 $M_\odot$, while the outer layers are ejected, essentially unaltered. The products of explosive silicon, oxygen, neon, and carbon burning are discussed in detail and compared with IR abundance observations. An agreement within the observational uncertainties is obtained. The comparison of predicted values for [O/Fe], [Ne/Fe], [Mg/Fe], [Si/Fe], [S/Fe], and [Ca/Fe] with those observed in low-metallicity stars with [Fe/H] < -1, which are expected to represent the average SN II production in the early galaxy before SN I's could contribute, shows that only the values of [O/Fe] through [Si/Fe] can be matched. This is due to the small mass of explosively processed matter inside 2 $M_\odot$. It is expected that higher mass stars with larger central density concentrations eject more processed material and lead to an average over the inital mass function, which can also reproduce the ratios of [S/Fe] and [Ca/Fe].

When excluding nonspherical effects in the explosion, we do not expect *r*-process nucleosynthesis to occur in a 20 $M_\odot$ supernova. In fact, the observed amount of stable Ni in the IR limits the amount of ejected neutron-rich matter to a minimum value, even for electron abundances as large as $Y_e = 0.494$, which are not at all neutron-rich enough to produce *r*-process nuclei. The constraints from radioactive ^{56}Ni, which powers the light curve at late times, and the observed amount of stable Ni determine the explosion energy *and* the mass cut between the neutron star and the ejecta. We conclude that an explosion energy of slightly more than 10^{51} ergs is required and a value of the mass cut of $M = 1.6 \pm 0.045\ M_\odot$. The sensitivity of the amount of stable Ni to the position of the mass cut lets us to expect a large variety of Ni/Fe ratios in different SN remnants, with larger ratios for lower mass remnants.

Long-lived radioactive nuclei like ^{56}Co, ^{57}Co, and ^{44}Ti will determine the late light curve and are produced in amounts of 0.07, 3.23×10^{-3}, and $1.23 \times 10^{-4}\ M_\odot$. They also lead to observable gamma transitions which will provide a further test also of the isotopic abundances produced in SN 1987A.

The mass cut of $M_b = 1.6 \pm 0.045\ M_\odot$ (baryonic) relates to a neutron star mass of $M_g = 1.43 \pm 0.05\ M_\odot$, after subtraction of the neutron star binding energy. When including uncertainties in the stellar model, the lower limit does not change, based on the present oxygen observations of SN 1987A. If future observations would reduce the mass estimate for oxygen, the progenitor's mass and thus the mass of the neutron star could be smaller. The upper limit can be increased to $M_b = 1.7\ M_\odot$ and $M_g = 1.52\ M_\odot$, when considering uncertainties in the 20 $M_\odot$ presupernova model. This upper limit is somewhat uncertain, because similar calculations for slightly larger masses (still covered by the uncertainty range for the progenitor of SN 1987A) are not available. If the observed pulsar period of 0.5 ms would be confirmed and is due to rotation, this will set—together with the mentioned neutron star masses—severe limits to the nuclear equation of state, requiring a very soft EOS in between the ones by Canuto and Chitre (1974) and Arponen (1972).

This research was supported in part by NSF grant AST 87-03535, NASA grant NGR 22-007-272, the Grant-in-Aid for Scientific Research of the Ministry of Education, Science, and Culture in Japan (63302015, 01540216, 01652503), and the U.S.–Japan Cooperative Science Program (INT 88-15999), operated by the NSF and the Japanese Society for the Promotion of Science. The computations were performed at the National Center for Supercomputer Applications at the University of Illinois (AST 890009N). We acknowledge fruitful discussions with and comments from M. Aufderheide, E. Baron, T. Beers, K. Brecher, A. Burrows, A. G. W. Cameron, J. Cooperstein, J. Cowan, J. Danziger, D. Hartmann, R. Henry, J. Lattimer, G. Mathews, F. Matteucci, R. Mönchmeyer, E. Müller, P. Pinto, and S. Woosley. M. H. would like to thank M. Cassé, C. Césarsky, and J. P. Chiéze for their hospitality at CEN Saclay and CEA Bruyeres-le-Chatel.

REFERENCES

Aitken, D. K., Smith, C. H., James, S. D., Roche, P. F., Hyland, A. R., and McGregor, P. J. 1988, *M.N.R.A.S.*, **235**, 19P.
Alastuey, A., and Jancovici, B. 1978, *Astr. Ap.*, **266**, 1034.
Arnett, W. D. 1987, *Ap. J.*, **319**, 136.
Arnett, W. D., and Fu, A. 1989, *Ap. J.*, **340**, 396.
Arnett, W. D., Schramm, D. N., and Truran, J. W. 1989, *Ap. J. (Letters)*, **339**, L25.
Arnett, W. D., and Thielemann, F.-K. 1985, *Ap. J.*, **295**, 589.

© American Astronomical Society • Provided by the NASA Astrophysics Data System

1990ApJ...349..222T

Arponen, J. 1972, *Nucl. Phys.*, **A191**, 257.
Bao, Z. Y., and Käppeler, F. 1987, *Atomic Nucl. Data Tables*, **36**, 411.
Barkat, Z., and Wheeler, J. C. 1988, *Ap. J.*, **322**, 247.
Beers, T., Preston, G. W., and Schechtman, S. A. 1990, in preparation
Bethe, H. A., and Johnson, M. 1974, *Nucl. Phys.*, **A230**, 1.
Bethe, H. A., and Wilson, J. 1985, *Ap. J.*, **295**, 14.
Bionta, R. M., *et al.* 1987, *Phys. Rev. Letters*, **58**, 1494.
Blake, J. B., Woosley, S. E., Weaver, T. A., and Schramm, D. N. 1981, *Ap. J.*, **248**, 315.
Bregman, J. D., Axelrod, T. S., Cohen, M., Pinto, P. A., Rank, D. M., Witteborn, F. C., and Wooden, D. H. 1989, *Ap. J.* (*Letters*), submitted.
Bruenn, S. W. 1989*a*, *Ap. J.*, **340**, 955.
———. 1989*b*, *Ap. J.*, **341**, 385.
Burrows, A. 1988, *Ap. J.*, **334**, 891.
Burrows, A., and Lattimer, J. M. 1983, *Ap. J.*, **270**, 735.
Cameron, A. G. W. 1989, in *Cosmic Abundances of Matter*, ed. J. Waddington (AIP Conf. Proc. 183) (New York: AIP), p. 349.
Canuto, V., and Chitre, S. M. 1974, *Phys. Rev.*, **D9**, 1587.
Carbon, D. F., Barbuy, B., Kraft, R. P., Friel, E. D., and Suntzeff, N. B. 1987, *Pub. A.S.P.*, **249**, 674.
Cassatella, A. 1987, in *Proc. ESO Workshop on SN 1987A*, ed. I. J. Danziger (Garching: ESO), p. 101.
Caughlan, G. R., and Fowler, W. A. 1988, *Atomic Nucl. Data Tables*, **40**, 283.
Caughlan, G. R., Fowler, W. A., Harris, M. J., and Zimmerman, G. E. 1985, *Atomic Nucl. Data Tables*, **32**, 197.
Cooperstein, J., and Baron, E. 1989, in *Supernovae*, ed. A. Petschek (New York: Springer-Verlag), in press.
Cook, W. R., *et al.* 1988, *Ap. J.* (*Letters*), **334**, L87.
Cowan, J. J., Cameron, A. G. W., and Truran, J. W. 1983, *Ap. J.*, **265**, 429.
Danziger, I. J., Bouchet, P., Gouiffes, C., and Lucy, L. 1989, in preparation.
Danziger, I. J., Bouchet, P., Gouiffes, C., and Rufener, F. 1988, in *Big Bang, Active Galactic Nuclei, and Supernovae*, ed S. Hayakawa, K. Sato (Tokyo: Universal Academic Press), p. 143.
Domogatsky, G. V., and Nadyozhin, D. K. 1977, *M.N.R.A.S.*, **178**, 33P.
Epstein, R. I., Colgate, S. A., and Haxton, W. C. 1988, *Phys. Rev. Letters*, **61**, 2038.
Erickson, E. F., Haas, M. R., Colgan, S. W. J., Lørd, S. D., Burton, M. G., Wolf, J., Hollenbach, D. J., and Werner, M. 1988, *Ap. J.* (*Letters*), **330**, L39.
Filippone, B. W., Humblet, J., and Langanke, K. 1989, *Phys. Rev. C.*, **40**, 515.
Fowler, W. A., Caughlan, G. E., and Zimmerman, B. A. 1975, *Ann. Rev. Astr. Ap.*, **13**, 69.
François, P. 1986, *Astr. Ap.*, **160**, 264.
———. 1987, *Astr. Ap.*, **176**, 294.
Friedman, J. L., Ipser, J. R., and Parker, L. 1986, *Ap. J.*, **304**, 115.
———. 1989, *Phys. Rev. Letters*, **62**, 3015.
Fu, A., and Arnett, W. D. 1989, *Ap. J.*, **340**, 414.
Fuller, G. M., Fowler, W. A., and Newman, M. 1980, *Ap. J. Suppl.*, **42**, 447.
———. 1982, *Ap. J. Suppl.*, **48**, 279.
———. 1985, *Ap. J.*, **293**, 1.
Gehrels, N., Leventhal, M., and MacCallum, C. J. 1988, in *Nuclear Spectroscopy of Astrophysicial Sources* (AIP Conf. Proc. 170), p. 87.
Gehren, T. 1988, *Rev. Mod. Astr.*, **1**, 52.
Graboske, H. C., DeWitt, H. E., Grossman, A. S., and Cooper, M. S. 1973, *Ap. J.*, **181**, 457.
Grebenev, S. A., and Sunyaev, R. A. 1988, *Soviet Astr. Letters*, **14**, 675.
Gratton, R., and Sneden, C. 1987, *Astr. Ap.*, **178**, 179.
Hartmann, K., and Gehren, T. 1988, *Astr. Ap.*, **199**, 269.
Hashimoto, M., and Nomoto, K. 1989, in preparation
Hashimoto, M., Nomoto, K., and Shigeyama, T. 1989, *Astr. Ap.*, **210**, L5. (Paper I).
Haxton, W. C. 1988, *Phys. Rev. Letters*, **60**, 1999.
Henry, R. B. C., and Fesen, R. A. 1988, *Ap. J.*, **329**, 693.
Hillebrandt, W., Höflich, P., Truran, J. W., and Weiss, A. 1987, *Nature*, **327**, 597.
Hillebrandt, W., Klapdor, H. V., Oda, T., and Thielemann, F.-K. 1981, *Astr. Ap.*, **99**, 195.
Hirata, K., *et al.* 1987, *Phys. Rev. Letters*, **58**, 1490.
Höflich, P. 1988, in *IAU Colloquium 108, Atmospheric Diagnostics of Stellar Evolution*, ed. K. Nomoto (Berlin: Springer), p. 288.
Iben, I., and Tutukov, A. V. 1984, *Ap. J. Suppl.*, **54**, 335.
———. 1985, *Ap. J. Suppl.*, **58**, 661.
Itoh, N., Totsuji, H., Ichimaru, S., and DeWitt, H. E. 1979, *Ap. J.*, **234**, 1079; erratum *Ap. J.*, **239**, 415.
Kettner, K. U., *et al.* 1982, *Zs. Phys.*, **A308**, 73.
Kirshner, R. P. 1988, in *IAU Colloquium 108, Diagnostics of Stellar Evolution*, ed. K. Nomoto (Berlin: Springer-Verlag), p. 252.
Klapdor, H. V., Oda, T., Metzinger, J., Hillebrandt, W., and Thielemann, F.-K. 1981, *Zs. Phys.*, **A299**, 213.
Kremer, M. U., *et al.* 1988, *Phys. Rev. Letters*, **60**, 14475.
Kristian, J., *et al.* 1989, *Nature*, **338**, 234.
Kudritzki, R. P., Groth, H. G., Butler, K., Husfeld, D., Becker, S., Eber, F., and Fitzpatrick, E. 1987, in *SN 1987 A*, ed. I. J. Danziger (Garching: ESO), p. 39.
Kumagai, S., Shigeyama, T., Nomoto, K., Itoh, M. Nishimura, J., and Tsuruta, S. 1989, *Ap. J.*, **345**, 412.
Lattimer, J. M., Mackie, F., Ravenhall, D. G., and Schramm, D. N. 1977, *Ap. J.*, **213**, 225.
Lattimer, J. M., and Yahil, A. 1989, *Ap. J.*, **340**, 426.
LeBlanc, J. M., and Wilson, J. R. 1970, *Ap. J.*, **161**, 541.
Lederer, C. M., and Shirley, V. S. 1978, *Table of Isotopes* (New York: Wiley-Interscience).
Luck, R. E., and Bond, H. E. 1985, *Ap. J.*, **292**, 559.
Maeder, A. 1987, *Astr. Ap.*, **173**, 247.
Magain, P. 1987, *Astr. Ap.*, **179**, 176.
Mahoney, W. A., *et al.* 1988, *Ap. J.* (*Letters*), **334**, L81.
Mathews, G. J., Bazan, G., and Cowan, J. J. 1990, in preparation.
Mathews, G. J., and Cowan, J. J. 1989, in *Heavy Ion Physics and Nuclear Astrophysical Problems*, ed. S. Kubono, M. Ishihara, and T. Nomura (Singapore: World Scientific), p. 143.
Matteucci, F. 1987, in *Stellar Evolution and Dynamics of the Outer Halo of the Galaxy*, ed. M. Azzopardi, and F. Matteucci (ESO Conf. Proc. 27) (Garching: ESO), p. 609.
Matteucci, F., and François, P. 1989, *M.N.R.A.S.*, **239**, 885.
Matz, S. M., Share, G. H., Leising, M. D., Chupp, E. L., Vestrand, W. T., Purcell, W. R., Strickman, M. S., and Reppin, C. 1988, *Nature*, **331**, 416.
Mayle, R. W., and Wilson, J. R. 1988, *Ap. J.*, **334**, 909.
Mönchmeyer, R. 1989, Ph.D. thesis, Technische Universität, Munchen.
Myra, E. S., and Bludman, S. 1989, *Ap. J.*, **340**, 384.
Nomoto, K., and Hashimoto, M. 1988, *Phys. Rep.*, **163**, 13.
Nomoto, K., Hashimoto, M., Shigeyama, T., and Kumagai, S. 1988, *Proc. Astr. Soc. Australia*, **7**, 490.
Nomoto, K., Shigayama, T., and Hashimoto, M. 1987, in *SN 1987A*, ed. I. J. Danziger (Garching: ESO), p. 325.
Nomoto, K., Thielemann, F.-K., and Yokoi, K. 1984, *Ap. J.*, **286**, 644.
Pandharipande, V. R., and Smith, R. A. 1975, *Nucl. Phys.*, **A175**, 225.
Phillips, M. M. 1988, private communication.
Rank, D. M., Pinto, P. A., Woosley, S. E., Bregman, J. D., Witteborn, F. C., Axelrod, T. S., and Cohen, M. 1989, *Nature*, **331**, 505.
Redder, A., *et al.* 1987, *Nucl. Phys.*, **A462**, 3995.
Renzini, A., and Voli, M. 1981, *Astr. Ap.*, **94**, 175.
Saio, H., Kato, M., and Nomoto, K. 1988, *Ap. J.*, **331**, 388.
Sandie, W. G., *et al.* 1988, *Ap. J.* (*Letters*), **334**, L91.
Shapiro, S. L., and Teukolsky, S. A. 1983, *Black Holes, White Dwarfs, and Neutron Stars* (New York: Wiley).
Shigeyama, T., Nomoto, K., and Hashimoto, M. 1988, *Astr. Ap.*, **196**, 141.
Shigeyama, T., Nomoto, K., Hashimoto, M., and Sugimoto, D. 1987, *Nature* **328**, 320.
Symbalisty, E. M. D., Schramm, D. N., and Wilson, J. R. 1985, *Ap. J.* (*Letters*), **291**, L11.
Taylor, J., and Weisberg, J. 1989, preprint.
Teegarden, B. J., Barthelmy, S. D., Gehrels, N., Tueller, J., Leventhal, M., and MacCallum, C. J. 1989, *Nature*, **339**, 122.
Terndrup, D. M., *et al.* 1988, *Proc. Astr. Soc. Australia*, **7**, 412.
Thielemann, F.-K., and Arnett, W. D. 1985, *Ap. J.*, **295**, 604.
Thielemann, F.-K., Arnould, M., and Hillebrandt, W. 1979, *Astr. Ap.*, **74**, 175.
Thielemann, F.-K., Arnould, M., and Truran, J. W. 1987, in *Advances in Nuclear Astrophysics*, ed. E. Vangioni-Flam *et al.* (Gif sur Yvette: Editions Frontieres), p. 525.
Thielemann, F.-K., Nomoto, K., and Yokoi, K. 1986, *Astr. Ap.*, **158**, 17.
Tomkin, J., and Lambert, P. L. 1984, *Ap. J.*, **279**, 220.
Tomkin, J., Sneden, C., and Lambert, P. L. 1986, *Ap. J.*, **302**, 415.
Truran, J. W., Cowan, J. J., and Cameron, A. G. W. 1978, *Ap. J.* (*Letters*), **22**, L63.
Truran, J. W., and Weiss, A. 1987, in *Nuclear Astrophysics*, ed. W. Hillebrandt, R. Kuhfuß, E. Müller, and J. W. Truran, *Lecture Notes in Physics*, Vol. **287**, (Berlin: Springer-Verlag), p. 283.
Tuchman, Y., and Wheeler, J. C. 1989, preprint.
Wagoner, R. V. 1969, *Ap. J. Suppl.*, **18**, 247.
Wagoner, R. V., Fowler, W. A., and Hoyle, F. 1967, *Ap. J.*, **148**, 3.
Weaver, T. A., and Woosley, S. E. 1980, *Ann. NY Acad. Sci.*, **366**, 335.
Weiss, A. 1989, *Ap. J.*, **339**, 365.
Wiescher, M. 1989, private communication.
Wiescher, M., Görres, J., Graaf, S., Buchmann, L., and Thielemann, F.-K. 1989, *Ap. J.*, **343**, 352.
Wiescher, M., Görres, J., and Thielemann, F.-K. 1988, *Ap. J.*, **326**, 384.
Wiescher, M., Görres, J., Thielemann, F.-K., and Ritter, H. 1986, *Astr. Ap.*, **160**, 56.
Wiescher, M., Harms, V., Görres, J., Thielmann, F.-K., and Rybarcyk, L. J. 1987, *Ap. J.*, **316**, 162.
Wheeler, J. C., Sneden, C., and Truran, J. W. 1989, *Ann. Rev. Astr. Ap.*, **27**, 279.
Wilson, J. R. 1985, in *Numerical Astrophysics*, ed. J. Centralla, J. LeBlanc, and R. Bowers (Boston: Jones and Bartlett), p. 422.
Wilson, J. R., and Mayle, R. W. 1988, *Phys. Rep.*, **163**, 63.
Wilson, J. R., Mayle, R., Woosley, S. E., and Weaver, T. A. 1986, in *Proc. 12th Texas Symposium on Relativistic Astrophysics, Ann. NY Acad. Sci.*, **470**, 267.
Witteborn, F. C., Bregman, J. D., Wooden, D. H., Pinto, P. A., Rank, D. M., Woosley, S. E., and Cohen, M. 1989, *Ap. J.* (*Letters*), **338**, L9.
Woosley, S. E. 1988, *Ap. J.*, **330**, 218.
Woosley, S. E., Arnett, W. D., and Clayton, D. D. 1973, *Ap. J. Suppl.*, **26**, 231.
Woosley, S. E., Axelrod, T. S., and Weaver, T. A. 1984, in *Stellar Nucleosynthesis*, ed. C. Chiosi and A. Renzini (Dordrecht: Reidel), p. 263.
Woosley, S. E., and Chevalier, R. A. 1989, *Nature*, **338**, 321.
Woosley, S. E., Fowler, W. A., Holmes, J. A., and Zimmerman, B. A. 1979, *Atomic Nucl. Data Tables*, **22**, 371.

© American Astronomical Society • Provided by the NASA Astrophysics Data System

1990ApJ...349..222T

Woosley, S. E., Hartmann, D., Hoffman, R. B., and Haxton, W. C. 1990, preprint.
Woosley, S. E., and Haxton, W. C. 1988, *Nature*, **334**, 45.
Woosley, S. E., Pinto, P. A., and Ensman, L. 1988, *Ap. J.*, **324**, 466.
Woosley, S. E., Pinto, P. A., and Hartmann, D. 1989, preprint.
Woosley, S. E., Pinto, P. A., and Weaver, T. A. 1988, *Proc. Astr. Soc. Australia*, **7**, 355.
Woosley, S. E., and Weaver, T. A. 1986, *Ann. Rev. Astr. Ap.*, **24**, 205.
———. 1988, *Phys. Rep.*, **163**, 79.

MASA-AKI HASHIMOTO: Institut d'Astrophysique de Paris, 98 bis, Boulevard Arago, F-75014 Paris, France

KEN'ICHI NOMOTO: Departmant of Astronomy, University of Tokyo, Bunkyo-ku, Tokyo 113, Japan

FRIEDRICH-KARL THIELEMANN: Harvard-Smithsonian Center for Astrophysics, 60 Garden Street, Cambridge, MA 02138

© American Astronomical Society • Provided by the NASA Astrophysics Data System